A key role for p60-Katanin in axon navigation is conditioned by the tubulin polyglutamylase TTLL6

Daniel Ten Martin[1], Nicolas Jardin[1], François Giudicelli[2#], Laïla Gasmi[1], Juliette Vougny[3], Cécile Haumaître[4], Xavier Nicol[3], Carsten Janke[5,6], Coralie Fassier[*,1,3,†,$] and Jamilé Hazan[*,1,†]

1. Sorbonne Université, INSERM U1130, CNRS UMR8246, Neuroscience Paris Seine - Institut de Biologie Paris-Seine (NPS-IBPS), F-75005 Paris, France

2. Sorbonne Université, CNRS UMR7622, Biologie du Développement Paris Seine - Institut de Biologie Paris-Seine (LBD-IBPS), F-75005 Paris, France

3. Sorbonne Université, INSERM, CNRS, Institut de la Vision, F-75012 Paris, France

4. Université Paris Diderot, INSERM UMR1149, ERL CNRS 8252, F-75018 Paris, France

5. Institut Curie, PSL Research University, CNRS UMR3348, F-91405 Orsay, France

6. Université Paris Sud, Université Paris-Saclay, CNRS UMR3348, F-91405 Orsay, France

* These authors contributed equally.

† Correspondence should be addressed to JH (e-mail: jamile.hazan@upmc.fr) or CF (e-mail: coralie.fassier@inserm.fr).

$ CF current address: Sorbonne Université, INSERM UMR_S968, CNRS UMR_7210, Institut de la Vision, Paris, France.

FG current address : Institut de Biologie de l'École Normale Supérieure, ENS, CNRS UMR8197, INSERM U1024.

Running title: Katanin and TTLL6 in axon navigation

Keywords: p60-katanin/ spastin/ microtubule-severing enzymes/ axon pathfinding / TTLL enzymes / microtubule polyglutamylation/ zebrafish

Word count: 7135

Abstract

Selective interplay between microtubules and their regulatory proteins emerged as major regulator of neuronal circuit development. However, how microtubule posttranslational modifications influence this interplay to govern axon guidance and targeting remains elusive. Using loss-of-function and rescue experiments during zebrafish development, we show that the microtubule-severing enzyme p60-Katanin controls motor axon pathfinding and larval mobility in a dose-dependent manner, and plays non-overlapping roles with the related protein Spastin in these processes. Notably, we uncover the tubulin glutamylase TTLL6 as a selective and key regulator of p60-Katanin activity during axon navigation. In contrast, our study demonstrates that, although critical for motor circuit wiring, the highly similar glutamylase TTLL11 fails to influence p60-Katanin and to rescue the axon targeting errors associated with TTLL6 knockdown, which discloses the functional specificity of these long-chain glutamylases at a physiological level. Altogether, our work provides *in vivo* proofs of concept that the tubulin code acts in a highly selective manner to tune the activity of key microtubule-severers in neuronal circuit wiring of a vertebrate model.

Introduction

Over the past decades, the microtubule (MT) cytoskeleton has emerged as a key player in nervous system development. MTs indeed provide mechanical support rails for axonal transport as well as mediate key signalling events that contribute to the morphological and behavioural changes that neurons undergo during neural circuit wiring, from neuron polarisation to synapse formation (Conde and Caceres, 2009; Hoogenraad and Bradke, 2009; Dent *et al*., 2011). The instructive role of microtubules in axon navigation processes was initially suggested by live imaging studies on cultured neurons showing that asymmetric invasion and stabilization of MTs in filopodia predicted growth cone turning and directionality (Williamson et *al*., 1996; Zhou et *al*., 2002). These analyses were further supported by the work of Buck and Zheng (2002), who demonstrated that stabilising or destabilizing MTs on one side of a growth cone was sufficient to induce growth-cone turning *in vitro*. MT dynamics and growth directionality within growth cones were shown to be influenced *in vitro* by guidance cues such as Netrin-1, Semaphorin-3a, Wnt3a or Wnt5a (Dent *et al*., 2004; Purro *et al*., 2008; Qu *et al*., 2013; Li *et al*., 2014; Shao *et al*., 2017; Biswas and Kalil, 2018). Concomitantly, several MT-interacting proteins were identified as major players in growth-cone decision-making behaviours at axon guidance choice points during vertebrate or invertebrate embryogenesis (Rothenberg *et al*., 2003; Lee *et al*., 2004; Del Rio *et al*., 2004; Lewcock *et al*., 2007; Arbeille and Bashaw, 2018; Fassier *et al*., 2018; Jardin et al., 2018; Slater *et al*., 2019).

While these data illustrated the importance of the MT cytoskeleton in axon navigation, the molecular mechanisms underpinning the fine-tuned remodelling of this network that drive growth cone steering is far from being understood. Neuronal MT dynamics are regulated by a myriad of proteins, including MT-severing enzymes

that control MT mass/number by promoting MT disassembly or amplification depending on the dynamic state of the newly severed ends (McNally and Roll-Mecak, 2018). Katanin was the first MT-severing enzyme to be identified (Hartmann *et al*., 1998) and purified (McNally and Vale, 1993): it is a heterodimer composed of a regulatory subunit of 80 kDa (p80-katanin) and a catalytic subunit of 60 kDa (p60-katanin). Since its discovery, katanin was shown to play a central role in neurogenesis, neuronal morphogenesis, migration and plasticity (Sharp and Ross, 2012; Eom *et al*., 2014; Mishra-Gorur *et al*., 2014; Jiang *et al*., 2017; Lombino *et al*., 2019). Notably, p60-katanin - the subunit that bears the MT-severing activity - was shown to be required for axon extension of zebrafish primary motor neuron (pMN) *in vivo* (Butler *et al*., 2010) and axon outgrowth and branching of mammalian neurons *in vitro* (Ahmad *et al*., 1999, Karabay *et al*., 2004; Yu *et al*., 2008). Consistently, in developing rodent neurons, p60-katanin is highly enriched during axon outgrowth but drastically drops as axons reach their target cells (Karabay *et al*., 2004). These expression data prompted us to examine whether p60-katanin influences growth cone directional steering and targeting *in vivo* as hypothesized by Vitriol and Zheng (2012).

MT-severing enzymes are regulated by tubulin posttranslational modifications (PTM) (Roll-Mecak, 2020; Janke and Magiera, 2020). In particular, tubulin polyglutamylation, a complex PTM, which is abundant in neurons (Audebert *et al*., 1994) and catalysed by the tubulin tyrosine ligase-like (TTLL) enzymes (van Dijk *et al*., 2007), promotes MT severing by spastin and p60-katanin *in vitro* (Lacroix *et al*., 2010; Valenstein and Roll-Mecak., 2016; Shin *et al*., 2019). Moreover, the MT-severing activity of spastin is finely regulated by the number of glutamates on the tubulin tails (Valenstein and Roll-Mecak, 2016). Yet, to precisely unravel the influence and selectivity of tubulin glutamylation upon different MT-severing-driven

physiological processes, analyses of the interplays between specific tubulin glutamylases and MT severing enzymes remained to be undertaken *in vivo*.

We here address this issue by (i) exploring the role of p60-Katanin in zebrafish motor circuit wiring with respect to its highly related severer spastin, and (ii) investigating whether the long chain tubulin glutamylases TTLL6 and TTLL11 that are both expressed in the teleost developing spinal cord (Pathak *et al*., 2011), may selectively tune p60-Katanin activity in this process. Using loss-of-function and rescue approaches, we uncover a key role for p60-Katanin in motor axon targeting and larval locomotion and establish its non-overlapping function with Spastin in this process. We further show that the zebrafish long-chain tubulin-glutamylase TTLL6 and TTLL11 play crucial but distinct roles in motor axon targeting, and reveal TTLL6-mediated tubulin polyglutamylation as a selective regulator of p60-Katanin activity in navigating axons. Our data thus provide the first *in vivo* evidence that the tubulin code acts in a highly selective manner to fine-tune the activity of key neuronal MT severers during nervous system development.

Materials and Methods

Zebrafish maintenance

Zebrafish embryos (*Danio rerio*) were obtained from natural spawning of wild-type, *p60-katanin* mutants (*katna1*^{sa18250}; Sanger Centre, purchased from the ZIRC) or transgenic Tg(*Hb9*:GFP) (Flanagan-Steet *et al*., 2005), Tg(*Hb9*:Gal4) (Zelenchuk and Brusés, 2011), and the newly generated Tg(*UAS*:Spastin-HA) lines. All embryos were maintained at 28°C in E3 medium (5 mM NaCl, 0.17 mM KCl, 0.33 mM $CaCl_2$, 0.33 mM $MgSO_4$, 0.00001% (w/v) Methylene Blue) and staged by hours post-fertilisation (hpf) and gross morphology according to Kimmel *et al*. (1995). To prevent pigment formation, 0.2 mM of 1-phenyl-2-thiourea (PTU, Sigma) was added to the E3 media from 24 hours post-fertilisation (hpf) onwards.

All our experiments were made in agreement with the European Directive 210/63/EU on the protection of animals used for scientific purposes, and the French application decree 'Décret 2013-118'. The fish facility has been approved by the French 'Service for animal protection and health', with the approval number A-75-05-25.

Generation of transgenic Tg(*UAS*:Spastin-HA) fish

As thoroughly described in Jardin *et al*. (2018) for the two transgenic lines selectively expressing the long or the short Spastin isoform, the transgenic Tg(*UAS*:Spastin-HA) line that express both isoforms was generated from a cDNA construct combining the three elements below in the following order: (i) a SacII-SwaI fragment of plasmid 'T2 US E1B Cit UAS E1B MCS ACR' (kind gift from Sebastian Gerety and David Wilkinson) composed of an 'alpha-crystallin:mRFP' cassette for screening purposes due to its specific expression in the lens, (ii) a SwaI-AvrII fragment from a UAS expression vector (Baraban *et al*., 2013) allowing specific

expression of the transgene in GAL4-expressing cells, and (iii) a SpeI-NotI fragment containing the full-length HA-tagged *spastin* cDNA followed by the SV40 3'UTR and polyadenylation signal of the pCS2+ vector. The resulting construct was cloned into pBluescrit SKI-SceI (Grabher *et al*., 2004), which was injected at 30pg/egg into freshly fertilised eggs together with I-SceI endonuclease (Roche) and 0.5% phenol red in 1X I-SceI digestion buffer (New England Biolabs). Injected fish were raised to adulthood and screened for germline transmission by detecting red fluorescence at 72 hpf in the lens of their progeny, which formed the transgenic Tg(*UAS*:Spastin-HA) line.

Genomic DNA isolation and genotyping

Genomic DNA was isolated by incubating larval heads 2 hours at 55°C in lysis buffer (100mM Tris Hcl, 2mM EDTA pH8, 0.2% Triton X-100, 250 µg/mL proteinase K). Homozygous and heterozygous *katna1*mutants were identified by PCR amplification followed by DNA sequencing (GENEWIZ). The primers used for genotyping were the following:

Katna1sa18250_FOR: 5'-GTAGTACGGAAATCCTCTGTCC-3'

Katna1sa18250_REV: 5'-TTGCTTTGATCTAAGAAACCGG-3'.

RNA extraction and RT-PCR analysis

For sequence analysis of *katna1* mRNA, total mRNA of 24-hpf *katna1*$^{+/+}$ and maternal zygotic *katna1*$^{-/-MZ}$ zebrafish embryos were extracted with Trizol according to the manufacturer's instructions. *Katna1* transcripts were reverse-transcribed and PCR-amplified using the SuperScript™ III One-Step RT-PCR System with

Platinum® Taq (ThermoFisher Scientific, Illkirch, France) from 200 ng of *katna1*$^{+/+}$ and *katna1*$^{-/-MZ}$ RNA extracts using the following primers:

Katna1RTPCRex3-4_FOR: 5'-ATGTGGAGCACAGATCGTCTCCATGTG-3'

Katna1RTPCRex5-6_REV: 5'-CAGCAATGTCATCCCATGTGACATTGGG-3'.

For quantitative RT-PCR analysis of *katna1* homologous gene expression levels, RNAs were extracted from 5 independent pools of 10 *katna1*$^{+/+}$, 10 *katna1*$^{-/-MZ}$ and one pool of 10 wild-type embryos (24 hpf) using the RNeasy Mini-kit (Qiagen, Courtaboeuf, France) and reverse-transcribed using the Superscript RT II Kit with random hexamers (Invitrogen, ThermoFisher Scientific, Illkirch, France). qPCR was performed using a SYBR Green master mix (EurobioGreen qPCR Mix, Hi-ROX; Eurobio Scientific, Courtaboeuf, France) using the primers listed in Table 1. The relative quantification method was used to calculate the expression levels of the genes of interest normalized to *lsmb12* and relative to the cDNAs from 24-hpf wild-type embryos. Values are shown as means ± SEM.

Whole-mount *in situ* hybridization

A 3'-fragment of *katna1* cDNA was isolated from a collection of 24-hpf zebrafish embryo mRNAs using the SuperScript® III One-Step RT-PCR system (Invitrogen) with the following forward and reverse primers: 5'-AGAGTGGATTTACTCAAGATCAACC-3' and 5'-AAGCTTGACTTGTACGCAGTGAACC-3'. The RT-PCR product was cloned into the TOPO® TA cloning pcr4 vector (Invitrogen) and sequenced. The *katna1* digoxigenin-labelled sense and antisense riboprobes were synthetized from the linearised recombinant TOPO® TA cloning vector using T7 and T3 RNA Polymerase (Promega) according to the supplier's instructions. Whole-mount *in situ* hybridisation

experiments were performed at 18 and 24 hpf using standard procedures (Macdonald *et al*., 1994). Pictures were acquired with a binocular stereomicroscope (Leica M165C) combined with an HD camera (Leica IC80 HD), then adjusted for brightness and contrast with the NIH Image J software.

Morpholinos and RNA injections

Morpholino oligonucleotides (MO) blocking *p60-katanin/katna1, ttll6, ttll11* or *spastin* translation initiation sites as well as the standard control MO were developed by GeneTools (Philomath, USA) and designed as follows:

MO^{ctl}: 5'-CCTCTTACCTCAGTTACAATTTATA-3',

MO^{p60Kat}: 5'-CTCATTGATCTCCCCCAAACTCATC-3',

$MO^{katna1aug1}$: 5'-CATCCTGTAAGTTAAAGTGGTCAGT-3' (Butler *et al*., 2010),

MO^{TTLL6} : 5'-CTGGTGTCCCCATTCTGATCTCTTC-3' (Pathak *et al*., 2011) and

MO^{TTLL11} : 5'-CGGCTGATTTGTTATCTCATCTAGG-3',

$MOsp^{ATG1}$: 5'-ATTCATTCACCCTTCTCGGGCTCTC-3' (Jardin *et al*., 2018),

$COMOsp^{ATG1}$: 5'-ATTGATTCAGCCTTGTCGCGCTGTC-3' (Jardin *et al*., 2018).

MO^{p60Kat} was injected at 1.3 and 3.4 pmol/embryo, $MO^{katna1aug1}$ at 0.9 pmol/embryo, MO^{TTLL6} at 0.2 pmol/embryo, MO^{TTLL11} at 0.8 pmol/embryo, $MOsp^{ATG1}$ and $COMOsp^{ATG1}$ at 0.4 pmol/embryo. Universal control MO^{ctl} morpholino was injected at all these doses depending on the controlled knockdown experiment. All morpholinos were injected at two-cell stage. Human full-coding *KATNA1* cDNA was isolated from a human fetal brain Marathon-ready cDNA collection (Clontech, Invitrogen) with the following forward and reverse primers: 5'-ATATAGGATCCATGTACCCATACGATGTTCCAGATTACGCTAGTCTTCTTATGATTAGTGAG-3' and 5'-

ATATATCTAGATTAGCATGATCCAAACTCAAATATC-3', and subsequently cloned into pCS2+ BamH1/XbaI restriction sites for rescue experiments. Zebrafish *spastin* full-length cDNA was amplified and HA-tagged by PCR from the IMAGE clone BG728071 with 5'-ATACTCGAGCAAGCTTGATTTAGGTGA-3' forward and 5'-GGCTCTAGATCAAGCGTAGTCAGGCACGTCGTAAGGGTAACTAGCGCCTACGCCAGTCGTGTCTCCGT-3' reverse primers, and cloned into pCS2+ using the XhoI/XbaI restriction sites included in the primers. Human *KATNA1*, mouse *TTLL6* and *TTLL11* (cDNAs provided by C Janke), as well as zebrafish *spastin* mRNAs were *in vitro* transcribed from the corresponding linearized pCS2+ constructs using SP6 mMessage mMachine kit (Ambion) and injected at one-cell stage. For rescue experiments, *KATNA1* mRNA was injected at 120 or 180 pg/embryo, *spastin* transcript at 150 pg/embryo, and both *TTLL6* and *TTLL11* at 120 pg/embryo.

Touch-evoked escape response test and manual tracking

To assess the motor behaviour of control, mutant, morphant and rescued 72-hpf larvae, we performed a touch response test by applying a tactile stimulus with a pair of forceps and analysing the larval escape behaviour under a Leica M165 C binocular stereomicroscope equipped with a Leica IC80 HD camera. Swimming speed and covered distance of each larva were quantified using the Manual Tracking plugin included in the Fiji software as reported in Fassier *et al*. (2010).

Whole-mount immunohistochemistry

Zebrafish embryos were fixed in PBS/4% paraformaldehyde during 2 hours at room temperature, washed 3 times with PBT1% (1% Triton X-100 in PBS) and

permeabilised using a 0.25% trypsin solution (Gibco) at 25°C when embryos were older than 24 hpf. Embryos were then blocked for two hours in PBT1% supplemented with 10% normal goat serum and incubated with primary antibodies overnight at 4°C in PBT1%/1% normal goat serum. The following primary antibodies were used: Znp-1 (1/100; ZIRC, University of Oregon), Zn-5 (1/200; ZIRC, University of Oregon) and GFP (1/1000; Molecular Probes). After several washes in PBT1%, embryos were incubated overnight at 4°C with the appropriate secondary antibody (Alexa Fluor 488 or 555 at 1/1000, Molecular Probes).

For glutamylated Tubulin staining, embryos were fixed in Dent's fixative (80% Methanol/20% DMSO) overnight at 4°C. After rehydration in regressive methanol/PBS-0.5% Tween 20®, embryos were blocked in PBT1% supplemented with 1% DMSO, 1% bovine serum albumin and 5% normal goat serum, and sequentially incubated with primary antibodies, GT335 (1:1000, Adipogen) and PolyE (1:1200; provided by C. Janke), and adequate secondary antibodies. Images were acquired using a fluorescence microscope equipped with an Apotome module (Zeiss, Axiovert 200M), a 20x objective (NA 0.5), the AxioCam MRm camera (Zeiss) and the Axiovision software (Zeiss). Images were processed with the NIH Image J software. Each figure panel corresponds to a projection image from a z-stack of 2-µm sections.

Time-lapse videomicroscopy assay

Control and MO^{p60Kat}-injected Tg(*Hb9*:GFP) embryos were anesthetised with E3 medium containing tricaine and embedded in 0.8% low-melting agarose in a 35-mm glass dish (Iwaki). Time-lapse videomicroscopy recording of spinal motor axon outgrowth was carried out at 28°C in E3 medium (supplemented with tricaine) using a

Leica DMI 6000B inverted spinning-disk microscope with a 40x immersion objective (NA 1.4) and a 491-nm 100-mW Cobolt calypso laser over 30 hours. Embryos immobilised at 22 hpf were filmed with a 20x immersion objective over 48 hours. In both cases, z-stacks of 80-µm-thick sections were acquired every 8 minutes with a step size of 1 µm using an EMCCD camera (Photometrics Quantem 512 SC) and the Metamorph software (Molecular Devices) and compiled into time-lapse movies.

Statistical Analysis

All data were obtained from at least two to three independent experiments. Statistical significance of the data was evaluated using the non-parametric Mann-Whitney test when comparing two groups assuming non-Gaussian distributions. The Kruskal–Wallis ANOVA test with Dunn's post-test or the One-Way ANOVA test with Bonferroni's post-test were used when comparing more than two groups assuming non-Gaussian or Gaussian distribution, respectively. Data distribution was tested for normality using the D'Agostino and Pearson normality test. All Statistical analyses were performed using GraphPad Prism 5.00 (GraphPad Software, San Diego, CA).

Results

p60-Katanin knockdown alters zebrafish spinal motor axon outgrowth and pathfinding in a dose-dependent manner

A morpholino-based functional screening aiming at identifying key MT-severing enzymes in zebrafish motor circuit wiring revealed the influence of both Spastin and p60-Katanin in this process. Consistently, p60-Katanin transcript is markedly expressed in the zebrafish developing spinal cord at embryonic stages where primary (18 somites) and secondary (24-26 hpf) motor axons initiate their outgrowth into the periphery (Fig. S1). To explore the role of zebrafish p60-Katanin in motor axon navigation, we performed *in toto* immunohistochemistry and *in vivo* live imaging experiments in wild-type or Tg(*Mnx1*:GFP) embryos (i.e., expressing the GFP in motor neurons) injected with different doses (1.3 or 3.4 pmol/embryo) of p60-Katanin (MO^{p60Kat}) or control (MO^{Ctl}) morpholinos. These analyses showed that p60-Katanin knockdown affected both pMN and sMN axon targeting in a dose-dependent manner (Figs. 1 & 2). Indeed, while low doses of MO^{p60Kat} ($MO^{p60Kat/1.3\ pmol}$) elicited aberrant branching of ventrally projecting pMN (CaP) axons compared to MO^{Ctl} (arrowheads, Fig. 1A-B), higher doses of MO^{p60Kat} ($MO^{p60Kat/3.4\ pmol}$) significantly impaired their outgrowth compared to CaP axons from both MO^{Ctl} and $MO^{p60Kat/1.3\ pmol}$ embryos (asterisks, Fig. 1A-C). The different pMN axon phenotypes of $MO^{p60Kat/1.3\ pmol}$ and $MO^{p60Kat/3.4\ pmol}$ embryos were equally rescued by injecting proportional doses (120 or 180 pg/embryo) of human *KATNA1* mRNA (Fig. 1A-C). Moreover, the analysis of sMN axons also revealed different axon pathfinding defects between these two sets of morphants (i.e., embryos injected with MO^{p60Kat}). Some dorsal motor nerves of $MO^{p60Kat/1.3\ pmol}$ larvae appeared abnormally split in distinct fascicles and mistargeted (empty arrows, Fig. 2A-B) compared to control dorsal

nerves (full arrows, Fig. 2A-B and Movies 1, 2). In contrast, the vast majority of dorsal nerves failed to form in $MO^{p60Kat/3.4\ pmol}$ larvae compared to MO^{Ctl} and $MO^{p60Kat/1.3\ pmol}$ (Fig. 2A,C) larvae. Furthermore, $MO^{p60Kat/3.4\ pmol}$ morphants, and to a lesser extent $MO^{p60Kat/1.3\ pmol}$ larvae, showed misrouted rostral nerves that were aberrantly targeted caudally (empty arrowheads, Fig. 2A,D and Movie 4); this phenotype was barely observed in control larvae (full arrowheads, Fig. 2A-D and Movie 3). Moreover, a significant number of $MO^{p60Kat/3.4\ pmol}$ larvae (57%) exhibited sMN axons that exited the spinal cord at ectopic sorting points (asterisks, Fig. 2A,E), compared to $MO^{p60Kat/1.3\ pmol}$ (10%) and MO^{Ctl} larvae (3%). Similar axon pathfinding defects were observed following the injection of the p60-Katanin morpholino ($MO^{katna1aug1}$) used in Butler *et al*. (2010), strengthening the phenotypic specificity (Fig. S2). Notably, the sMN axon targeting errors of both $MO^{p60Kat/1.3\ pmol}$ and $MO^{p60Kat/3.4\ pmol}$ larvae were fully rescued by injecting proportional doses of human *KATNA1* mRNA (Fig. 2A-E), which confirmed that these axon pathfinding defects were specifically due to a dose-dependent lack of p60-Katanin.

Altogether, our data show that p60-Katanin controls vertebrate motor axon navigation in a dose-dependent manner, in addition to its well-defined role in axon extension.

P60-Katanin and Spastin play distinct roles in spinal motor axon targeting

Zebrafish p60-Katanin and Spastin were suggested to have different but related functions in pMN axon outgrowth (Butler *et al*., 2010). To support this paradigm, we showed that the respective depletion of either p60-Katanin or Spastin causes different sMN defects including the abnormal splitting of the dorsal nerve (Fig. 2A) or the ectopic sorting of motor neuron somata from the spinal cord (Jardin et *al*.,

2018). However, both morphants also exhibited overlapping sMN axon pathfinding defects (e.g., the aberrant caudal targeting of the rostral nerve) that could reflect functional redundancy. To assess the specificity of these closely related MT-severing enzymes in motor neuron development, we conducted cross-rescue analyses. We showed that ubiquitous overexpression of human spastin (i.e., injection of 150 pmol of human spastin-encoding *SPG4* mRNA in 1-cell stage morphant embryos) failed to rescue the branching and pathfinding defects of both pMN (Fig. 3A-B) and sMN (Fig. 3A,C-D) axons from $MO^{p60Kat/1.3pmol}$ morphants unlike human p60-katanin overexpression (Figs. 1 & 2). Conversely, the same dose of human *SPG4* mRNA efficiently rescued the pathfinding errors of zebrafish *spastin* morphants (Jardin *et al*., 2018). Likewise, ubiquitous overexpression of human p60-katanin (using the same dose of *KATNA1* mRNA as that injected to rescue *p60-katanin* morphant phenotypes) failed to alleviate the axon targeting defects of Spastin-depleted pMN (Fig. S3A) and sMN axons (Fig. S3B-C). To strengthen these results, we conducted motor neuron-targeted cross-rescue experiments using the *UAS*/GAL4 system. To this aim, we injected 1.3 pmol of *p60-katanin* morpholino in double Tg(*Hb9*:GAL4;*UAS*:Spastin-HA) transgenic embryos that mosaically expressed an HA-tagged version of zebrafish Spastin in spinal motor neurons. Again, CaP axons of $MO^{p60Kat/1.3pmol}$-injected Tg(*Hb9*:Gal4;*UAS*:Spastin-HA) embryos appeared twice more branched than control Tg(*Hb9*:GAL4;*UAS*:Spastin-HA) axons, whether they overexpressed Spastin (HA+; red arrowheads; Fig. 3E-F) or not (HA^-; yellow arrowheads; Fig. 3E-F). However, it should be noted that the expression of Spastin-HA in sMN from $MO^{p60Kat/1.3pmol}$-injected Tg(*Hb9*:GAL4;*UAS*:Spastin-HA) larvae was too mosaic to assess its impact on dorsal and rostral nerve targeting.

These data demonstrate that p60-Katanin and Spastin play non-overlapping roles in vertebrate motor axon outgrowth, branching and targeting.

p60-Katanin knockdown causes severe deficit in larval mobility

We next investigated the functional consequences of the morphant axon pathfinding defects on larval locomotion using a touch-evoked escape response test. Morphant larvae injected with 1.3 or 3.4 pmol of MO^{p60Kat} had a curved-tail phenotype, which was more penetrant with increasing doses of morpholinos (Movies 5, 6, 8). Furthermore, both types of morphants showed a striking loss of motility compared to control larvae, although they clearly responded to touch stimulation (Fig. 4A and Movies 5, 6, 8). Both $MO^{p60Kat/1.3pmol}$ and $MO^{p60Kat/3.4pmol}$ morphants indeed swam over shorter distances (Fig. 4B) and at a slower speed (Fig. 4C) than control larvae. The injection of 120 pg of human *KATNA1* transcript in $MO^{p60Kat/1.3pmol}$ morphants (or 180 pg of human KATNA1 mRNA in $MO^{p60Kat/3.4pmol}$ morphants) suppressed the curved-tail phenotype and locomotor deficit of these two sets of mophants (Fig. 4A-C and Movies 5-9), unlike the injection of zebrafish *spastin*/*spg4* mRNA (Fig. 4A-C and Movie 10). These rescue assays are totally consistent with the rescue of the pMN and sMN axon targeting defects described in Figs 1 & 2. Altogether, these data ascertain a specific role for p60-Katanin in zebrafish motor circuit wiring and larval locomotor behaviour.

***katna1* mutant show similar morphological, behavioural and motor axon pathfinding defects to *p60-katanin* morphants**

To validate the specificity of the p60-Katanin morphant phenotypes, we undertook the characterisation of the $katna1^{sa18250}$ mutant from the Sanger Centre

(hereafter called *katna1* mutant). This zebrafish ENU mutant harboured a point mutation (G>A) in the donor splice site of *katna1* intron 4 (Fig. 5A). Both zygotic (*katna1*$^{-/-Z}$) and maternal zygotic (*katna1*$^{-/-MZ}$) mutants developed normally (unlike *p-80 katanin* mutants; Hu *et al*., 2014), with the exception of 23% of them showing a curved-tailed phenotype (Fig. 5B-C) like *p60-katanin* morphants (Movie 6). Moreover, *katna1*$^{-/-MZ}$ larvae at 6-days post-fertilisation (dpf) showed defective inflation of the swimming bladder, a gas-filled organ that regulates buoyancy and is essential for survival in most teleost species (Fig. S4). To test the consequences of the *katna1*^{sa18250} mutation on mRNA splicing, we undertook RT-PCR analyses. They showed that these mutants lacked wild-type *katna1* transcript but expressed mis-spliced transcripts with aberrant insertions of different-sized intron-4 fragments, which all led to a frameshift and the appearance of a premature STOP codon at the same amino-acid position (Fig. 5D-F). This truncating mutation depleted a large portion of the protein including the ATPase domain, suggesting that homozygous *katna1* mutants are null mutants. We next assessed the locomotor behaviour of 72-hpf *katna1*$^{-/-MZ}$ mutants using the touch-evoked escape response test. Following touch stimulation, *katna1*$^{-/-MZ}$ mutants showed an altered startle response, which was characterised by a reduced swimming speed and, to a lesser extent, shorter swimming distances (Fig. 5G-H). This locomotor deficit was associated with robust defects of sMN axon pathfinding, including the abnormal splitting of the dorsal nerves (white arrows, Fig. 5I-K) and, less frequently, the caudal misrouting of the rostral nerves (Fig. S5). Notably, the percentage of heterozygous versus homozygous mutant larvae with dorsal or rostral nerve defects (Figs. 5J and S5), as well as the number of misguided dorsal and rostral projections per *katna1*$^{+/-}$ and *katna1*$^{-/-Z}$ larva (Figs. 5K

and S5) confirmed the dose effect of p60-Katanin on motor axon targeting, as revealed by the morphant analysis.

Although less severely affected, *katna1*$^{-/-Z}$ and *katna1*$^{-/-MZ}$ mutants recapitulated the morphological, behavioural and axon pathfinding defects of *p60-katanin* morphants. These combined results thus ruled out the possibility of non-specific effects due to morpholino injection or ENU mutagenesis. Interestingly, RT-qPCR analysis of the expression level of mRNAs encoding p60-Katanin-related proteins from the meiotic clade of ATPases (Monroe *et al*., 2016) revealed a significant increase in the transcript levels of two MT-severing enzymes, Spastin (*spast*), and Fidgetin (*fign*), and a *katna1* paralogue, Katanin-like 2 (*katnal2*), in *katna1*$^{-/-MZ}$ embryos compared to controls (Fig. 5L). This analysis suggests that genetic compensation by some *katna1*-related genes, like *katnal2* or *fign*, may account for the milder phenotype of *katna1* null mutants.

Knockdown of MT glutamylases TTLL6 and TTLL11 affects spinal motor axon targeting

Since p60-Katanin and Spastin have non-overlapping roles in motor circuit wiring (Fig. 4 and Fig. S3), we assessed whether the functional specificity of these two MT-severing enzymes could be underlain by their preference for distinct populations of MTs. We chose to focus on Tubulin glutamylation, a MT post-translation modifications (PTM) which was known to be enriched in all neuronal compartments (Janke and Kneussel, 2010) and to promote spastin and katanin-mediated MT-severing *in vitro* (Sharma *et al*., 2007; Lacroix *et al*., 2010; Valenstein and Roll-Mecak, 2016, Shin *et al*., 2019). Notably, long-chain-generating glutamylases, TTLL6 and TTLL11 were shown to influence the activity of spastin,

and to a lesser extent of katanin, in non-neuronal cells (Lacroix *et al*., 2010). The enrichment of *ttll6* and *ttll11* trancripts in the zebrafish developing spinal cord at stages of motor axon outgrowth (Pathak *et al*., 2011) prompted us to examine whether these two enzymes could be involved in this developmental process. We first verified the presence of polyglutamylated MTs in zebrafish spinal motor axons with two antibodies recognizing both long and short chains of glutamates (GT335) or long chains only (polyE). Glutamate side chains were detected in both pMN axons at 26 hpf and sMN tracts at 72 hpf (Fig. 6A-B). To investigate the role of this PTM in motor circuit wiring, we carried out loss-of-function analyses of TTLL6 and TTLL11 glutamylases using morpholinos targeted against their translation initiation site (MO^{TTLL6} and MO^{TTLL11}). *TTLL6* and *TTLL11* morphants were indistinguishable in terms of gross morphology as both showed a ventrally curved body axis at 72 hpf (Fig. 6C, upper panels). This morphological phenotype was previously associated with ciliary defects in *TTLL6* morphants (Pathak *et al*., 2011) and could suggest a similar involvement of *TTLL11* in zebrafish cilium biogenesis and/or motility. The analysis of pMN and sMN axon outgrowth and targeting in these two sets of morphants revealed substantial differences (Fig. 6C middle and bottom panels). While *TTLL11* and *TTLLL6* knockdown equally led to aberrant branching of ventrally projecting pMN axons (i.e., CaP axons; arrows, Fig. 6C-D), only the depletion of TTLL11 significantly impaired their elongation compared to control CaP axons (asterisks, Fig. 6C,E). Moreover, TTLL6-depleted larvae showed a significant number of split and misguided dorsal nerves (empty arrows, Fig. 6C) compared to control larvae (full arrows, Fig. 6C,F), as described for $MO^{p60Kat/1.3pmol}$ larvae (Fig. 2). In contrast, numerous dorsal tracts were missing in *TTLL11* morphants compared to *TTLL6* morphants and controls (Fig. 6C,H). Furthermore, while 25% and 19% of

sMN rostral projections were abnormally targeted caudally in *TTLL6* and *TTLL11* morphants (empty arrowheads, Fig. 6C,G), rostral nerves of TTLL11-depleted larvae appeared mostly defasciculated (bracket, Fig. 6C), which was barely observed in *TTLL6* morphant and control larvae (Fig. 6C,I). Furthermore, *TTLL11* (97%) and to a lesser extent *TTLL6* morphants (33%) showed sMN axons that exited the spinal cord at ectopic sorting points (asterisks, middle and bottom panels, Fig. 6C,J), as well as misrouted sMN somata that abnormally emigrated from the spinal cord (14% and 47% of the morphant larvae, respectively; yellow arrows, bottom panels; Fig. 6C,K). These two phenotypes were never observed in control larvae (Fig. 6C,J-K). Notably, similar migratory defects of sMN somata were described as a characteristic feature of *spastin* morphants and mutants (Jardin *et al*., 2018).

Although partially overlapping, the motor neuron phenotypes of *TTLL6* and *TTLL11* morphants suggested that these two as yet indistinguishable polyglutamylases could differentially regulate motor circuit wiring. Furthermore, the significant phenotypic similarities associated with *TTLL6* or *TTLL11* knockdown and the depletion of p60-Katanin or Spastin hinted at a functional relationship between Tubulin glutamylation and MT severing in vertebrate motor axon targeting.

TTLL6 and TTLL11 have related but distinct functions in motor axon outgrowth and navigation

To assess the specificity of *TTLL6* and *TTLL11* morphant phenotypes and to clarify the functional selectivity or redundancy of these related enzymes, we carried out rescue and cross-rescue experiments by co-injecting MO^{TTLL6} or MO^{TTLL11} with 120 pg of mouse *TTLL6* or *TTLL11* transcripts. Notably, overexpression of mouse TTLL6 but not TTLL11 significantly alleviated the morphological and motor axon

outgrowth defects of *TTLL6* morphants (Fig. 7A, C-J). Reciprocally, overexpression of TTLL11 but not TTLL6 substantially rescued the morphological and pMN/sMN axon pathfinding defects of *TTLL11* morphants (Fig. 7B, C-J).

Overall, these analyses reveal that these two biochemically similar glutamylases play non-redundant key roles in zebrafish development, and specifically in spinal motor axon extension and navigation.

Only TTLL6-mediated MT polyglutamylation rescues the swimming deficit and motor axon targeting defects associated with p60-katanin partial knockdown

The overlapping phenotype between *p60-katanin* and *TTLL* morphants led us to hypothesize that at least one of these glutamylases could specifically enhance p60-Katanin activity during zebrafish motor circuit wiring. We thus assessed whether TTLL6 or TTLL11 overexpression could attenuate or rescue the larval locomotion deficit and motor axon pathfinding errors associated with the partial depletion of p60-Katanin (i.e., injection of 1.3 pmol of morpholino). Co-injection of 120 pg of mouse *TTLL6* transcript, but not *TTLL11* mRNA, fully restored the touch-induced escape behaviour (i.e., complete rescue of both the swimming speed and covered distances) of 72-hpf $MO^{p60Kat/1.3pmol}$ morphant larvae compared to controls (Fig. 8A-C). Consistently, overexpression of TTLL6 in $MO^{p60Kat/1.3pmol}$ embryos significantly reduced the number of supernumerary CaP axon branches (Fig. 8A,D) and respectively decreased by 58% and 60% the number of split/misrouted dorsal nerves and caudally targeted rostral nerves per larva (Fig. 8A,E-F). In contrast, TTLL11 overexpression failed to alleviate both pMN and sMN axon targeting defects of $MO^{p60Kat/1.3pmol}$ larvae (Figure 8A,D-F).

Altogether, these results provide the first *in vivo* proof of concept that selective modification of MT-glutamylation pattern by overexpression of a specific Tubulin glutamylase, herein TTLL6, can rescue the motor neuron and locomotor defects associated with p60-Katanin partial depletion.

TTLL6 selectively regulates p60-Katanin-driven motor axon targeting

TTLL6 overexpression in non-neuronal cells was shown to influence spastin severing activity (Lacroix *et al*., 2010). Furthermore, ectopic dendritic recruitment of TTLL6 induced by Tau missorting locally and specifically stimulated MT-severing by spastin in hippocampal neurons (Zempel *et al*., 2013). To test whether the rescue of $MO^{p60Kat/1.3pmol}$ morphant phenotypes by TTLL6 overexpression specifically relies on TTLL6-mediated stimulation of p60-Katanin remaining activity or involves other MT severing proteins (especially Spastin), we reproduced the same rescue experiments in a *p60-katanin* null mutant background (*katna1*$^{-/-MZ}$). We here showed that TTLL6 overexpression (as TTLL11 overexpression) failed to rescue the axon pathfinding errors and locomotor deficit of *katna1*$^{-/-MZ}$ mutants while a significant rescue of these phenotypes was obtained following human *KATNA1* overexpression (Fig. 9A-E). These results, which strikingly contrast with the beneficial impact of TTLL6 overexpression on $MO^{p60Kat/1.3pmol}$ morphants, ascertain the selectivity of TTLL6-mediated MT polyglutamylation as a regulator of p60-Katanin activity during motor axon targeting.

Discussion

Among the myriad of molecules shown to play prominent roles in axon guidance, special focus has been given to MT regulatory proteins due to their prominent roles in integrating and translating extracellular guidance signals into

changes in growth-cone morphology and behaviour (Lowery and Van Vactor, 2009; Dent *et al*., 2011; Kolodkin and Tessier-Lavigne, 2011).

p60-Katanin is required for accurate motor axon navigation

The MT-severing enzyme p60-katanin is known to be a decisive player in axon elongation (Ahmad *et al*., 1999; Karabay *et al*., 2004 Butler *et al*., 2010) and branching *(*Yu *et al*., 2008). Although enriched in mouse developing axons and growth cones during the whole outgrowth process (Karabay *et al*., 2004), the role of this MT-severer in axon steering had yet never been established. Using loss-of-function approaches during zebrafish embryogenesis, we have here unveiled a key role for p60-Katanin in spinal motor axon navigation and targeting. Intriguingly, p60-Katanin regulates this developmental process in a dose-dependent manner, emphasising the need of fine-tuning its activity *in vivo*. Interestingly, the orthologue of p60-katanin in the *Drosophila* exerts a MT-plus-end depolymerising activity *in vitro* in addition to its known severing activity (Zhang *et al*., 2011; Diaz-Valencia *et al*., 2011). The balance between these two functions seems to be influenced by its concentration, with the maximal depolymerisation rate occurring at a lower concentration than the maximal severing rate (Diaz-Valencia *et al*., 2011). This dual function of p60-katanin was reported to regulate MT dynamics at the actin cortex to fine-tune the cell migration of *Drosophila* S2 cells by suppressing protrusion. (Zhang *et al*., 2011). Thus, if applicable *in vivo* in a vertebrate model, this concentration-dependent versatile role of p60-katanin may provide an explanation for the dose-dependent effects of p60-Katanin depletion on axon outgrowth and targeting.

Furthermore, while we recently reported a role for Spastin in zebrafish motor axon pathfinding (Jardin *et al*., 2018), our cross-rescue experiments have here demonstrated that these two enzymes show non-overlapping functions in this process.

This is consistent with the observation that spastin and p60-katanin are differentially involved in MT remodelling in non-neuronal cells (Lacroix *et al*., 2010 and Shin *et al*., 2019) as well as in axon branch formation in cultured rodent hippocampal neurons (Yu *et al*., 2008). The functional specificity of these MT severers in axon branching has been previously linked to (**i**) their distinct subcellular distribution (with spastin being enriched at branch points) and (**ii**) the differential regulation of their severing activity by the MT-associated protein Tau, which more efficiently protects MTs from being severed by p60-katanin than by spastin (Qiang *et al*., 2006; Yu *et al*., 2008). While these mechanisms could also underlie their functional specificity in axon navigation, the present study provides compelling evidence for the central role of MT polyglutamylation in their differential regulation.

Along these lines, depletion of the two long-chain tubulin glutamylases TTLL6 or TTLL11 leads to motor axon targeting defects that are strikingly similar to those described for p60-Katanin (present study) and/or Spastin (Jardin *et al*., 2018) mutants and morphants. Furthermore, TTLL6-mediated polyglutamylation is here shown to a selective regulator of p60-Katanin-activity during motor axon targeting. Indeed, overexpression of TTLL6, but not TTLL11, rescues the axon pathfinding errors associated with p60-Katanin partial knockdown most likely by boosting the activity of residual p60-Katanin, as suggested by its lack of beneficial effect in p60-Katanin null mutants. Remarkably, interactions between the p60-katanin regulator Tau and MTs were shown to be sensitive to tubulin polyglutamylation levels *in vitro* (Boucher *et al*., 1994), as established for spastin and katanin MT-severing activities (Valenstein and Roll-Mecak, 2016; Shin *et al*., 2019). Overall, the model that emerges from all these observations is that MT polyglutamylation patterns by distinct glutamylases may selectively regulate the activity of MT-severing enzymes by

concomitantly (i) promoting their catalytic activity (i.e., increasing their coupling with the tubulin C-terminal tail, their hexamerization and ATPase activity; White *et al*., 2007; Valenstein *et al*., 2016; Shin *et al*., 2019; Zehr *et al*., 2020) and (ii) influencing the MT-binding affinity and/or activity of their regulators including Tau (Yu *et al*., 2008) and CRMPs (Ji *et al*., 2018).

However, beyond their molecular specificity, the characteristic axon pathfinding phenotypes due to the depletion of p60-Katanin or Spastin may also be the readout of their involvement in different axon guidance pathways. This was shown to be the case for M1 and M87/M61 Spastin main isoforms that were respectively identified as key effectors of BMP and Neuropilin-1 pathways in motor circuit wiring (Jardin *et al*., 2018). Interestingly, the regulatory p80-katanin subunit is required for Sonic hedgehog (Shh) signalling during neocortical development (Hu *et al*., 2014). Since we show that *katna1* mutants fail to inflate their swimming bladder, a process dependent on the Shh pathway (Winata *et al*., 2009), a role for p60-Katanin in Shh-mediated axon guidance (Yam and Charron, 2013) may be suggested.

Differential regulation of axon pathfinding by long-chain Tubulin glutamylases in vivo

Fine-tuning of MT dynamics and organisation is crucial for several cellular processes – including neuronal connectivity – and its dysfunction has been involved in an increasing number of human diseases (Gerdes and Katsanis, 2005; Breuss and Keays, 2014; Marchisella *et al*., 2016). Tubulin PTMs, including glutamylation, have been described as key mechanisms to generate sub-populations of MTs with distinct properties and cellular functionalities (Janke and Kneussel, 2010; Janke and Magiera, 2020). Based on their enzymatic specificity (addition of short or long glutamate side chains) and substrate preference (alpha- versus beta-subunit of tubulin dimers), TTLL

enzymes indeed catalyse different polyglutamylation patterns on MT outer surface (van Dijk *et al*., 2007). These distinct patterns were suggested to selectively and gradually fine-tune the activity of MT interactors including MT severers. However, cellular and physiological data confirming this selective regulation were still lacking until very recently. So far, excessive accumulation of neuronal tubulin glutamylation due to carboxypeptidase (CCP) depletion was shown to impair axonal transport and cause massive neurodegeneration in mice and humans (Magiera *et al*., 2018; Shashi *et al*., 2018). Recently, Bodakuntla *et al*. (2021) have shown that the axonal transport defects and Purkinje cell degeneration caused by CCP1-depletion-induced tubulin hyperglutamylation were selectively rescued by the knockout of the alpha-tubulin glutamylase TTLL1 but not by that of the beta-tubulin glutamylase TTLL7. This study thus confirms the relevance of the tubulin code in neuronal homeostasis. Revealing an additional level of complexity in the tubulin code, our study shows that two long chain tubulin glutamylases with similar substrate specificity (van Dijk *et al*., 2007) are not functionally redundant and differentially regulate the activity of key MT interactors (here p60-Katanin) in the development of vertebrate neuronal connectivity. Our results therefore imply that TTLL6 and TTLL11 may selectively fine-tune MT severers by generating distinct MT glutamylation patterns (i.e., the number of added glutamate residues, the precise targeted site...). Tackling the issue of the tubulin code specificity and its impact on key MT-dependent physiological processes will undoubtedly represent a major technological challenge for the forthcoming years.

In conclusion, our work reveals the key role of the MT-severing enzyme p60-Katanin and its selective control by MT polyglutamylation in motor axon navigation. By establishing the specific roles of two tubulin polyglutamylases in this developmental process, we show how subtle variations between tubulin-modifying

enzymes, which are not easily detectable by *in vitro* experiments, can lead to highly different functional readouts *in vivo*. Together with previous studies on the key role of MT tyrosination in the mouse developing brain (Erck *et al*., 2005; Marcos *et al*., 2009), our analysis reinforces the need to dissect the involvement of the tubulin-modifying enzymes in neuronal circuit wiring. One avenue of research would be to investigate the role of MT acetylation, which was shown to regulate p60-Katanin activity (Sudo and Baas, 2010; Mao *et al*., 2014), in axon guidance. Finally, dissecting the function and regulation of p60-Katanin *in vivo* may provide novel insight into the aetiology of human neurodevelopmental disorders caused by mutations disrupting the interactions between katanin regulatory (p80) and catalytic (p60) subunits (Hu *et al*., 2014; Mishra-Gorur *et al*., 2014).

Acknowledgements

We thank Sebastian Gerety and David Wilkinson for the 'alpha-crystallin:mRFP' plasmid used for screening our transgenic line, Susanne Bolte and Richard Schwartzman from the imaging facility of the "Institut de Biologie Paris Seine" (IBPS / Sorbonne University), Alex Bois, Stéphane Tronche and Aldelkrim Mannioui for fish care, as well as Amélie Fréal and Filippo Del Bene for fruitful comments.

Author Contribution

JH and CF designed the project and interpreted the data with DTM. DTM performed the functional analysis of p60-Katanin, TTLL6 and TTLL11 during zebrafish motor circuit development with the exception of live video-microscopy experiments, which were carried out by CF. CF performed all the experiments using the *katna1* mutant with the assistance of JV, and CH for RT-qPCR. NJ investigated the differential role of Spastin and p60-Katanin in spinal motor axon targeting and used the

Tg(*UAS*:Spastin-HA) transgenic line generated by CF and FG. LG provided technical assistance and developed various constructs. CF and JV are members of XN's lab and benefited from his experience in axon guidance processes. CJ performed TTLL cloning and had insightful comments throughout the study. JH and CF wrote the manuscript with the editing of CJ and FG.

Competing interests

The authors declare that they have no conflict of interest.

Funding

This work was supported by research grants to (i) JH from the Association Française contre les Myopathies (AFM), the Emergence Programme from the UPMC (University Paris 6) and the Association Strümpell-Lorrain (ASL)-HSP France and, (ii) to CF from the Association Strümpell-Lorrain (ASL)-HSP France (2015 and 2019), the Tom Wahlig Foundation grant (2019) and the Association Française contre les Myopathies (Grant 23695). CJ was supported by the ANR grant ANR-12-BSV2-0007. DTM was a recipient of a PhD fellowship from the "Ministère de l'Education Nationale, de la Recherche et de la Technologie".

References

Ahmad, F. J., Yu, W., McNally, F. J. and Baas, P. W. (1999). An essential role for katanin in severing microtubules in the neuron. *J. Cell Biol.* **145**, 305–315.

Arbeille, E. and Bashaw, G. J. (2018). Brain Tumor promotes axon growth across the midline through interactions with the microtubule stabilizing protein Apc2. *PLoS Genet.* **14**, e1007314.

Audebert, S., Koulakoff, A., Berwald-Netter, Y., Gros, F., Denoulet, P. and Eddé, B. (1994). Developmental regulation of polyglutamylated alpha- and beta-tubulin in mouse brain neurons. *J. Cell Sci.* **107**, 2313-2322.

Baraban, M., Anselme, I., Schneider-Maunoury, S. and Giudicelli, F. (2013). Zebrafish embryonic neurons transport messenger RNA to axons and growth cones in vivo. *J. Neurosci.* **33**, 15726–15734.

Biswas, S. and Kalil, K. (2018). The Microtubule-Associated Protein Tau Mediates the Organization of Microtubules and Their Dynamic Exploration of Actin-Rich Lamellipodia and Filopodia of Cortical Growth Cones. *J. Neurosci.* **38**, 291–307.

Bodakuntla, S., Yuan, X., Genova, M., Gadadhar, S., Leboucher, S., Birling, M.C., Klein, D., Martini, R., Janke, C. and Magiera, M.M. (2021). Distinct roles of α- and β-tubulin polyglutamylation in controlling axonal transport and in neurodegeneration. *EMBO J.* **40**, e108498.

Boucher, D., Larcher, J. C., Gros, F. and Denoulet, P. (1994). Polyglutamylation of tubulin as a progressive regulator of in vitro interactions between the microtubule-associated protein Tau and tubulin. *Biochemistry* **33**, 12471–12477.

Breuss, M. and Keays, D. A. (2014). Microtubules and neurodevelopmental disease: the movers and the makers. *Adv. Exp. Med. Biol.* **800**, 75–96.

Buck, K. B. and Zheng, J. Q. (2002). Growth cone turning induced by direct local modification of microtubule dynamics. *J. Neurosci.* **22**, 9358–9367.

Butler, R., Wood, J. D., Landers, J. A. and Cunliffe, V. T. (2010). Genetic and chemical modulation of spastin-dependent axon outgrowth in zebrafish embryos indicates a role for impaired microtubule dynamics in hereditary spastic paraplegia. *Dis. Model Mech.* **3**, 743–751.

Conde, C. and Cáceres, A. (2009). Microtubule assembly, organization and dynamics in axons and dendrites. *Nat. Rev. Neurosci.* **10**, 319–332.

Del Río, J. A., González-Billault, C., Ureña, J. M., Jiménez, E. M., Barallobre, M. J., Pascual, M., Pujadas, L., Simó, S., La Torre, A., Wandosell, F., *et al.* (2004). MAP1B is required for Netrin 1 signaling in neuronal migration and axonal guidance. *Curr. Biol.* **14**, 840–850.

Dent, E. W., Barnes, A. M., Tang, F. and Kalil, K. (2004). Netrin-1 and semaphorin 3A promote or inhibit cortical axon branching, respectively, by reorganization of the cytoskeleton. *J. Neurosci.* **24**, 3002–3012.

Dent, E. W., Gupton, S. L. and Gertler, F. B. (2011). The growth cone cytoskeleton in axon outgrowth and guidance. *Cold Spring Harb. Perspect. Biol.* **3**, a001800.

Díaz-Valencia, J. D., Morelli, M. M., Bailey, M., Zhang, D., Sharp, D. J. and Ross, J. L. (2011). Drosophila katanin-60 depolymerizes and severs at microtubule defects. *Biophys. J.* **100**, 2440–2449.

Eom, T.-Y., Stanco, A., Guo, J., Wilkins, G., Deslauriers, D., Yan, J., Monckton, C., Blair, J., Oon, E., Perez, A., *et al.* (2014). Differential regulation of microtubule severing by APC underlies distinct patterns of projection neuron and interneuron migration. *Dev. Cell* **31**, 677–689.

Erck, C., Peris, L., Andrieux, A., Meissirel, C., Gruber, A. D., Vernet, M., Schweitzer, A., Saoudi, Y., Pointu, H., Bosc, C., *et al.* (2005). A vital role of tubulin-tyrosine-ligase for neuronal organization. *Proc. Natl. Acad. Sci. U.S.A.* **102**, 7853–7858.

Fassier, C., Hutt, J. A., Scholpp, S., Lumsden, A., Giros, B., Nothias, F., Schneider-Maunoury, S., Houart, C. and Hazan, J. (2010). Zebrafish atlastin controls motility and spinal motor axon architecture via inhibition of the BMP pathway. *Nat. Neurosci.* **13**, 1380–1387.

Fassier, C., Fréal, A., Gasmi, L., Delphin, C., Ten Martin, D., De Gois, S., Tambalo, M., Bosc, C., Mailly, P., Revenu, C. *et al.* (2018). Motor axon navigation relies on Fidgetin-like 1-driven microtubule plus end dynamics. *J. Cell Biol.* **217**, 1719-1738.

Flanagan-Steet, H., Fox, M. A., Meyer, D. and Sanes, J. R. (2005). Neuromuscular synapses can form in vivo by incorporation of initially aneural postsynaptic specializations. *Development* **132**, 4471–4481.

Gerdes, J. M. and Katsanis, N. (2005). Small molecule intervention in microtubule-associated human disease. *Hum. Mol. Genet.* **14 Spec No. 2**, R291-300.

Grabher, C., Joly, J.-S. and Wittbrodt, J. (2004). Highly efficient zebrafish transgenesis mediated by the meganuclease I-SceI. *Methods Cell Biol.* **77**, 381–401.

Hartman, J. J., Mahr, J., McNally, K., Okawa, K., Iwamatsu, A., Thomas, S., Cheesman, S., Heuser, J., Vale, R. D. and McNally, F. J. (1998). Katanin, a microtubule-severing protein, is a novel AAA ATPase that targets to the centrosome using a WD40-containing subunit. *Cell* **93**, 277–287.

Hoogenraad, C. C. and Bradke, F. (2009). Control of neuronal polarity and plasticity--a renaissance for microtubules? *Trends Cell Biol.* **19**, 669–676.

Hu, W. F., Pomp, O., Ben-Omran, T., Kodani, A., Henke, K., Mochida, G. H., Yu, T. W., Woodworth, M. B., Bonnard, C., Raj, G. S., *et al.* (2014). Katanin p80 regulates human cortical development by limiting centriole and cilia number. *Neuron* **84**, 1240–1257.

Janke, C. and Kneussel, M. (2010). Tubulin post-translational modifications: encoding functions on the neuronal microtubule cytoskeleton. *Trends Neurosci*. **33**, 362–372.

Janke, C. and Magiera, M. M. (2020). The tubulin code and its role in controlling microtubule properties and functions. *Nat. Rev. Mol. Cell Biol*. **21**, 307–326.

Jardin, N., Giudicelli, F., Ten Martín, D., Vitrac, A., De Gois, S., Allison, R., Houart, C., Reid, E., Hazan, J. and Fassier, C. (2018). BMP- and neuropilin 1-mediated motor axon navigation relies on spastin alternative translation. *Development* **145**, dev162701.

Ji, Z., Zhang, G., Chen, L., Li, J., Yang, Y., Cha, C., Zhang, J., Lin, H. and Guo, G. (2018). Spastin Interacts with CRMP5 to Promote Neurite Outgrowth by Controlling the Microtubule Dynamics. *Dev. Neurobiol*. **78**, 1191-1205.

Jiang, K., Rezabkova, L., Hua, S., Liu, Q., Capitani, G., Altelaar, A.F.M., Heck, A.J.R., Kammerer, R.A., Steinmetz, M.O. and Akhmanova, A. (2017). Microtubule minus-end regulation at spindle poles by an ASPM-katanin complex. *Nat. Cell Biol*. **19**, 480-492.

Karabay, A., Yu, W., Solowska, J. M., Baird, D. H. and Baas, P. W. (2004). Axonal growth is sensitive to the levels of katanin, a protein that severs microtubules. *J. Neurosci*. **24**, 5778–5788.

Kimmel, C. B., Ballard, W. W., Kimmel, S. R., Ullmann, B. and Schilling, T. F. (1995). Stages of embryonic development of the zebrafish. *Dev. Dyn*. **203**, 253–310.

Kolodkin, A. L. and Tessier-Lavigne, M. (2011). Mechanisms and molecules of neuronal wiring: a primer. *Cold Spring Harb. Perspect. Biol*. **3**, a001727.

Lacroix, B., van Dijk, J., Gold, N. D., Guizetti, J., Aldrian-Herrada, G., Rogowski, K., Gerlich, D. W. and Janke, C. (2010). Tubulin polyglutamylation stimulates spastin-mediated microtubule severing. *J. Cell Biol*. **189**, 945–954.

Lee, H., Engel, U., Rusch, J., Scherrer, S., Sheard, K. and Van Vactor, D. (2004). The microtubule plus end tracking protein Orbit/MAST/CLASP acts downstream of the tyrosine kinase Abl in mediating axon guidance. *Neuron* **42**, 913–926.

Lewcock, J. W., Genoud, N., Lettieri, K. and Pfaff, S. L. (2007). The ubiquitin ligase Phr1 regulates axon outgrowth through modulation of microtubule dynamics. *Neuron* **56**, 604–620.

Li, L., Fothergill, T., Hutchins, B. I., Dent, E. W. and Kalil K. (2014). Wnt5a evokes cortical axon outgrowth and repulsive guidance by tau mediated reorganization of dynamic microtubules. *Dev. Neurobiol.* **74**, 797-817.

Lombino, F. L., Muhia, M., Lopez-Rojas, J., Brill, M. S., Thies, E., Ruschkies, L., Lutz, D., Richter, M., Hausrat, T. J., Lopes, A. T., *et al.* (2019). The Microtubule Severing Protein Katanin Regulates Proliferation of Neuronal Progenitors in Embryonic and Adult Neurogenesis. *Scientif. Rep.* **9**, 15940.

Lowery, L. A. and Van Vactor, D. (2009). The trip of the tip: understanding the growth cone machinery. *Nat. Rev. Mol. Cell Biol.* **10**, 332–343.

Macdonald, R., Xu, Q., Barth, K. A., Mikkola, I., Holder, N., Fjose, A., Krauss, S. and Wilson, S. W. (1994). Regulatory gene expression boundaries demarcate sites of neuronal differentiation in the embryonic zebrafish forebrain. *Neuron* **13**, 1039–1053.

McNally, F.J. and Vale, R.D. (1993). Identification of katanin, an ATPase that severs and disassembles stable microtubules. *Cell* **75**, 419-429.

McNally, F.J. and Roll-Mecak, A. (2018). Microtubule-severing enzymes : From cellular functions to molecular mechanism. *J. Cell Biol.* **217**, 4057-4069.

Magiera, M. M., Bodakuntla, S., Žiak, J., Lacomme, S., Marques Sousa, P., Leboucher, S., Hausrat, T. J., Bosc, C., Andrieux, A., Kneussel, M., *et al.* (2018).

Excessive tubulin polyglutamylation causes neurodegeneration and perturbs neuronal transport. *EMBO J*. **37**, e100440.

Mao, C.-X., Xiong, Y., Xiong, Z., Wang, Q., Zhang, Y. Q. and Jin, S. (2014). Microtubule-severing protein Katanin regulates neuromuscular junction development and dendritic elaboration in Drosophila. *Development* **141**, 1064–1074.

Marchisella, F., Coffey, E. T. and Hollos, P. (2016). Microtubule and microtubule associated protein anomalies in psychiatric disease. *Cytoskeleton (Hoboken)* **73**, 596–611.

Marcos, S., Moreau, J., Backer, S., Job, D., Andrieux, A. and Bloch-Gallego, E. (2009). Tubulin tyrosination is required for the proper organization and pathfinding of the growth cone. *PLoS ONE* **4**, e5405.

Mishra-Gorur, K., Çağlayan, A. O., Schaffer, A. E., Chabu, C., Henegariu, O., Vonhoff, F., Akgümüş, G. T., Nishimura, S., Han, W., Tu, S., *et al.* (2014). Mutations in KATNB1 cause complex cerebral malformations by disrupting asymmetrically dividing neural progenitors. *Neuron* **84**, 1226–1239.

Monroe, N. and Hill, C.P. (2016). Meotic Clade AAA ATPases: Protein Polymer Disassembly Machines. *J. Mol. Biol.* **14**, 1897-1911.

Pathak, N., Austin, C. A. and Drummond, I. A. (2011). Tubulin tyrosine ligase-like genes ttll3 and ttll6 maintain zebrafish cilia structure and motility. *J. Biol. Chem.* **286**, 11685–11695.

Purro, S. A., Ciani, L., Hoyos-Flight, M., Stamatakou, E., Siomou, E. and Salinas, P. C. (2008). Wnt regulates axon behavior through changes in microtubule growth directionality: a new role for adenomatous polyposis coli. *J. Neurosci.***28**, 8644–8654.

Qiang, L., Yu, W., Andreadis, A., Luo, M. and Baas, P. W. (2006). Tau protects microtubules in the axon from severing by katanin. *J. Neurosci.* **26**, 3120–3129.

Qu, C., Dwyer, T., Shao, Q., Yang, T., Huang, H. and Liu, G. (2013). Direct binding of TUBB3 with DCC couples netrin-1 signaling to intracellular microtubule dynamics in axon outgrowth and guidance. *J. Cell Sci.* **126**, 3070–3081.

Roll-Mecak, A. (2020). The tubulin code in microtubule dynamics and information encoding. *Dev. Cell* **54**, 7-20.

Rothenberg, M. E., Rogers, S. L., Vale, R. D., Jan, L. Y. and Jan, Y.-N. (2003). Drosophila pod-1 crosslinks both actin and microtubules and controls the targeting of axons. *Neuron* **39**, 779–791.

Shao, Q., Yang, T., Huang, H., Alarmanazi, F. and Liu, G. (2017). Uncoupling of UNC5C with Polymerized TUBB3 in Microtubules Mediates Netrin-1 Repulsion. *J. Neurosci*. **37**, 5620–5633.

Sharma, N., Bryant, J., Wloga, D., Donaldson, R., Davis, R. C., Jerka-Dziadosz, M. and Gaertig, J. (2007). Katanin regulates dynamics of microtubules and biogenesis of motile cilia. *J. Cell Biol*. **178**, 1065–1079.

Sharp, D. J. and Ross, J. L. (2012). Microtubule-severing enzymes at the cutting edge. *J. Cell Sci*. **125**, 2561–2569.

Shashi, V., Magiera, M. M., Klein, D., Zaki, M., Schoch, K., Rudnik-Schöneborn, S., Norman, A., Lopes Abath Neto, O., Dusl, M., Yuan, X., *et al.* (2018). Loss of tubulin deglutamylase CCP1 causes infantile-onset neurodegeneration. *EMBO J*. **37**, e100540.

Shin, S. C., Im, S.-K., Jang, E.-H., Jin, K. S., Hur, E.-M. and Kim, E. E. (2019). Structural and molecular basis for katanin-mediated severing of glutamylated microtubules. *Cell Rep*. **26**, 1357-1367.

Slater, P. G., Cammarata, G. M., Samuelson, A. G., Magee, A., Hu, Y. and Lowery, L. A. (2019). XMAP215 promotes microtubule-F-actin interactions to regulate growth cone microtubules during axon guidance in Xenopuslaevis. *J. Cell Sci*. **132**, jcs224311.

Sudo, H. and Baas, P. W. (2010). Acetylation of microtubules influences their sensitivity to severing by katanin in neurons and fibroblasts. *J. Neurosci.* **30**, 7215–7226.

Valenstein, M. L. and Roll-Mecak, A. (2016). Graded Control of Microtubule Severing by Tubulin Glutamylation. *Cell* **164**, 911–921.

van Dijk, J., Rogowski, K., Miro, J., Lacroix, B., Eddé, B. and Janke, C. (2007). A targeted multienzyme mechanism for selective microtubule polyglutamylation. *Mol. Cell* **26**, 437–448.

Vitriol, E. A. and Zheng, J. Q. (2012). Growth cone travel in space and time: the cellular ensemble of cytoskeleton, adhesion, and membrane. *Neuron* **73**, 1068–1081.

White, S.R., Evans, K.J., Lary, J., Cole, J.L. and Lauring, B. (2007). Recognition of C-terminal amino acids in tubulin by pore loops in Spastin is important for microtubule severing. *J. Cell Biol.* **176**, 995-1005.

Williamson, T., Gordon-Weeks, P. R., Schachner, M. and Taylor, J. (1996). Microtubule reorganization is obligatory for growth cone turning. *Proc. Natl. Acad. Sci. U.S.A.* **93**, 15221–15226.

Winata, C. L., Korzh, S., Kondrychyn, I., Zheng, W., Korzh, V. and Gong, Z. (2009). Development of zebrafish swimbladder: The requirement of Hedgehog

signaling in specification and organization of the three tissue layers. *Dev. Biol.* **331**, 222–236.

Yam, P. T. and Charron, F. (2013). Signaling mechanisms of non-conventional axon guidance cues: the Shh, BMP and Wnt morphogens. *Curr. Opin. Neurobiol.* **23**, 965–973.

Yu, W., Qiang, L., Solowska, J. M., Karabay, A., Korulu, S. and Baas, P. W. (2008). The microtubule-severing proteins spastin and katanin participate differently in the formation of axonal branches. *Mol. Biol. Cell* **19**, 1485–1498.

Zehr, E.A., Szyk, A., Szczesna, E., and Roll-Mecak, A. (2020). Katanin Grips the β-Tubulin Tail through an Electropositive Double Spiral to Sever Microtubules. *Dev. Cell* **52**, 118-131.

Zelenchuk, T. A. and Brusés, J. L. (2011). In vivo labeling of zebrafish motor neurons using an mnx1 enhancer and Gal4/UAS. *Genesis* **49**, 546–554.

Zempel, H., Luedtke, J., Kumar, Y., Biernat, J., Dawson, H., Mandelkow, E. and Mandelkow, E.M. (2013). Amyloid-beta oligomers induce synaptic damage via Tau-dependent microtubule severing by TTLL6 and spastin. *EMBO J.* **32**, 2920-2937.

Zhang, D., Grode, K. D., Stewman, S. F., Diaz-Valencia, J. D., Liebling, E., Rath, U., Riera, T., Currie, J. D., Buster, D. W., Asenjo, A. B., *et al.* (2011). Drosophila

katanin is a microtubule depolymerase that regulates cortical-microtubule plus-end interactions and cell migration. *Nat. Cell Biol.* **13**, 361–370.

Zhou, F.-Q., Waterman-Storer, C. M. and Cohan, C. S. (2002). Focal loss of actin bundles causes microtubule redistribution and growth cone turning. *J. Cell Biol.* **157**, 839–849.

Figure Legends

Figure 1. pMN axon outgrowth and branching are sensitive to p60-Katanin levels. (A) Immunolabelling of pMN axons in 26-hpf embryos injected with a control morpholino (MO^{Ctl}; n=32), 1.3 or 3.4 pmol of *p60-katanin* morpholino ($MO^{p60Kat/1.3pmol}$, n=32; $MO^{p60Kat/3.4pmol}$, n=32) or co-injected with the same two doses of *p60-katanin* morpholino and 120 (for $MO^{p60Kat/1.3pmol}$) or 180 (for $MO^{p60Kat/3.4pmol}$) pg of human *KATNA1* transcript ($MO^{p60Kat/1.3pmol}$ + $mRNA^{KATNA1}$, n=32; $MO^{p60Kat/3.4pmol}$ + $mRNA^{KATNA1}$, n= 32) using Znp-1 antibody. Lateral views of the trunk, anterior to the left. Arrowheads and asterisks respectively indicate hyper-branched and truncated CaP axons. Scale bar: 50µm. (B-C) Mean number of branches (B) and truncated CaP axons (C) per embryo. Quantifications were performed on 24 spinal cord hemisegments located around the yolk tube per embryo. Box and Whisker graphs. ***$p \leq 0.001$. Kruskal–Wallis ANOVA test with Dunn's post test. Whiskers indicate the Min/Max values.

Figure 2. *p60-katanin* knockdown markedly affects secondary motor axon targeting. (A) Immunolabelling of sMN tracts in 72-hpf Tg(*Hb9*:GFP) larvae injected with control morpholino (MO^{Ctl}; n=32), *p60-katanin* morpholino ($MO^{p60Kat/1.3pmol}$, n=32 and $MO^{p60Kat/3.4pmol}$, n=32) or co-injected with *p60-katanin* morpholino and human *KATNA1* mRNA ($MO^{p60Kat/1.3pmol}$ + $mRNA^{KATNA1}$, n=32; $MO^{p60Kat/3.4pmol}$ + $mRNA^{KATNA1}$, n=32) using Zn-5 and GFP antibodies. Lateral views of the trunk, anterior to the left. Right panels are higher magnifications of left panels. Dotted lines mark lateral myosepta. Full arrowheads and full arrows respectively show normal rostral and dorsal nerves. Empty arrowheads and empty arrows respectively indicate misguided rostral and dorsal projections. Asterisks point at aberrant exit points of sMN axons from the spinal cord. Scale bar (left panels): 50 μm. Scale bar (right

panels): 25 μm. (B-D) Mean number of misguided dorsal projections (B), missing dorsal projections (C) and misguided rostral nerves (D) per larva. Quantifications were performed on 24 spinal hemisegments around the yolk tube per larva. Box and Whisker graphs. *p≤ 0.05; **p≤ 0.01; ***p≤ 0.001; Kruskal–Wallis ANOVA test with Dunn's post test. Whiskers indicate the Min/Max values. (E) Percentage of larvae with ectopic sorting of sMN axons from the spinal cord. ***p≤ 0.001; Chi^2 test.

Figure 3. Ubiquitous or motoneuron-targeted overexpression of Spastin fails to rescue spinal motor axon defects of *p60-katanin* morphants. (A) Upper panels: Immunolabelling of pMN axons in 26-hpf wild-type embryos injected with a control morpholino (MO^{Ctl}; n= 30), 1.3 pmol of *p60-katanin* morpholino ($MO^{p60Kat\ /1.3pmol}$, n= 30) or co-injected with 1.3 pmol of MO^{p60Kat} and human spastin-encoding *SPG4* mRNA ($MO^{p60Kat\ /1.3\ pmol}$ + $mRNA^{Spast}$, n= 30) using Znp-1 antibody. Arrowheads point at supernumerary branches of CaP pMN axons. Middle and lower panels: Immunolabelling of sMN axons in 72-hpf Tg(*Hb9*:GFP) larvae injected with MO^{Ctl} (n= 10), 1.3 pmol of MO^{p60Kat} (n= 10) or co-injected with MO^{p60Kat} and human *SPG4* mRNA ($MO^{p60Kat\ /1.3\ pmol}$ + $mRNA^{Spast}$, n= 10) using Zn-5 and GFP antibodies. Dotted lines indicate lateral myosepta. Full arrowheads and full arrows respectively show normal rostral and dorsal nerves. Empty arrowheads and empty arrows respectively indicate misguided rostral and dorsal projections. All images are lateral views of the trunk, anterior to the left. Scale bars: 25 μm. (B-D) Mean number of CaP pMN branches (B), misguided/split dorsal nerves (C) and misguided rostral nerves (D) per embryo or larva. Quantifications were performed on 24 spinal hemisegments around the yolk tube per embryo (B) or larva (C-D). Box and Whisker graphs. ***p≤ 0.001;

ns: non-significant (p>0.05); Kruskal–Wallis ANOVA test with Dunn's post test (B, D) and One-way ANOVA with Bonferroni's post test (C). Whiskers indicate the Min/Max values. (E) Immunolabelling of pMNs in 26-hpf double transgenic Tg(*Hb9*:Gal4; *UAS*:Spastin-HA) embryos injected with a control morpholino or 1.3 pmol of *p60-katanin* morpholino using Znp-1 and HA antibodies. Empty white and pink arrowheads respectively point at spastin-HA-negative and -positive CaP axons of MO^{Ctl}- injected Tg(*Hb9*:Gal4;*UAS*:Spastin-HA) embryos. Yellow and red arrowheads respectively indicate spastin-HA-negative and -positive CaP axons of $MO^{p60Kat/1.3pmol}$-injected Tg(*Hb9*:Gal4;*UAS*:Spastin-HA) embryos. (F) Mean number of branches per 100 Spastin-positive and -negative CaP pMN axons in 26-hpf Tg(*Hb9*:Gal4;*UAS*:Spastin-HA) control and $MO^{p60Kat/1.3pmol}$-injected embryos. At least 100 neurons were analysed per condition. Box and Whisker graph. ***p≤ 0.001; ns: non-significant (p>0.05); Kruskal–Wallis ANOVA test with Dunn's post test. Whiskers indicate the Min/Max values.

Figure 4. Loss of p60-Katanin causes a dramatic decrease in zebrafish larval mobility. (A) Touch-evoked escape behaviour of 72-hpf larvae injected with a control morpholino (MO^{Ctl}; n= 90), increasing doses of *p60-katanin* morpholino ($MO^{p60Kat/1.3pmol}$; n=102 and $MO^{p60Kat/3.4\ pmol}$; n=85), or co-injected with MO^{p60Kat} morpholino and human *KATNA1* or zebrafish *spastin* mRNA ($MO^{p60Kat/1.3pmol}$ + $mRNA^{KATNA1}$, n= 91; $MO^{p60Kat/1.3pmol}$ + $mRNA^{Spast}$, n= 87; $MO^{p60Kat/3.4pmol}$ + $mRNA^{KATNA1}$, n= 97). Each line represents the trajectory of one larva after touch stimulation while the distance between two dots indicate the distance covered by a larva between two consecutive frames. Scale bar: 5mm. (B-C) Mean swimming distance (B) and speed (C). Box and Whisker graphs. ***p≤0.001; ns: non-significant

(p>0.05); Kruskal–Wallis ANOVA test with Dunn's post test. Whiskers indicate the Min/Max values.

Figure 5. Zebrafish *katna1* mutants show similar morphological, behavioural and motor axon targeting defects to *p60-katanin* morphants. (A) Sequence analysis of control and *katna1* mutant genomic DNA. Dotted line indicates the junction between exon 4 (pink background) / intron 4 (white background). The green arrowhead points at the nucleotide substitution affecting the donor splice site of intron 4 (G in control; black arrowhead) in *katna1* mutants (G>A). (B) Gross morphology of 72-hpf control (*katna1*$^{+/+}$) and *katna1* homozygous mutant (*katna1*$^{-/-}$) larvae. Arrows point at the curved-tail phenotype of some mutant larvae. Scale bar: 0.5 mm. (C) Percentage of control (+/+) and maternal zygotic *katna1* mutant (-/- *MZ*) larvae exhibiting a curved-tail phenotype. ***p≤0.001; Chi^2 test. (D) Schematic representation of the RT-PCR strategy used to test the impact of the *katna1* splice-site mutation on *katna1* mRNA splicing. Dotted lines indicate intron splicing. Arrows represent the primers used for RT-PCR analysis. Primers were designed on exon/intron junctions to avoid contamination by genomic DNA amplification. In: intron; Ex: exon. (E) RT-PCR analysis of *katna1* intron-4 splicing on total RNA extracts from *katna1*$^{+/+}$ and *katna1*$^{-/-}$ *MZ* embryos. Homozygous *katna1*$^{-/-}$ *MZ* embryos lack wild-type transcript and show different populations of mis-spliced transcripts (1, 2 and 3). (F) Sequence analysis of *katna1* mis-spliced transcripts. Sequences corresponding to exon 4, intron 4 and exon 5 are respectively indicated in pink, white and blue. The splice-site mutation is highlighted in green. Mis-spliced transcripts include various sized insertions of intron 4, which all lead to a frameshift and the occurence of a premature stop codon at the same amino-acid position (red

asterisk). (G-H) Mean swimming distance (G) and mean swimming speed (H) of 72-hpf *katna1*$^{+/+}$ and *katna1*$^{-/-}$ *MZ* larvae in a touch-evoked escape response test. Box and Whisker graphs. * p≤0.05; ***p≤0.001; Mann Whitney test. Whiskers indicate the Min/Max values. (I) Immunolabelling of sMN axons in 72-hpf controls (*katna1*$^{+/+}$, n=34), as well as heterozygous *katna1*$^{+/-}$, n=53), homozygous zygotic (*katna1*$^{-/-}$*Z*, n=33) and maternal zygotic (*katna1*$^{-/-}$ *MZ*, n=12) mutant larvae using Zn-5 antibody. Lateral views of the trunk, anterior to the left. Insets are higher magnifications of a dorsal nerve. Empty arrows point at split/misguided dorsal nerves. Scale bars: 25 μm, inset: 10 μm. (J) Percentage of larvae with dorsal nerve defects. **p≤0.01; ***p≤0.001; Chi^2 test. (K) Mean number of misguided dorsal projections. Box and Whisker graphs. ***p≤0.001; ns: non-significant; Kruskal–Wallis ANOVA test with Dunn's post test. Whiskers indicate the Min/Max values. (L) RT-qPCR analysis showing the differential expression levels of p60-Katanin-related genes from the Meiotic Clade ATPases in control and *katna1*$^{-/-}$ *MZ* larvae. * p≤0.05; **p≤0.01; ns: non-significant. Unpaired t-test.

Figure 6. *TTLL6* and *TTLL11* knockdown differentially affects spinal motor axon outgrowth and pathfinding. (A-B) Immunodetection of polyglutamylated microtubules (MTs) in 26- and 72-hpf wild-type embryos using GT335 (A) and poly E (B) antibodies that respectively label both short and long chains of glutamates or long chains only. Lateral views of the trunk, anterior to the left. Polyglutamylated MTs are observed in pMN (26 hpf) and sMN (72 hpf) axons. Scale bars: 25 μm. (C) Upper panels: Overall morphology of 72-hpf control (MO^{Ctl}), *TTLL6* (MO^{TTLL6}) and *TTLL1* (MO^{TTLL11}) morphant larvae. Both *TTLL6* and *TTLL11* morphants exhibit a severe ventrally curved body-axis phenotype compared to MO^{Ctl}-injected larvae.

Scale bars: 250 µm. Middle panels: Immunolabelling of pMNs in 26-hpf MO^{Ctl} (n= 30), MO^{TTLL6} (n= 30) and MO^{TTLL11} (n= 30) embryos using Znp-1 antibody. Arrows and asterisks respectively indicate hyper-branched and truncated CaP axons. Lower panels: Immunolabelling of sMN axons in 72-hpf Tg(*Hb9*:GFP) larvae injected with MO^{Ctl} (n= 30), MO^{TTLL6} (n= 30) or MO^{TTLL11} (n= 30) larvae. Dotted lines delineate lateral myosepta. Full arrowheads and full arrows respectively point at normal rostral and dorsal nerves. Empty arrowheads and empty arrows respectively indicate misguided rostral and dorsal projections. Brackets show defasciculated rostral nerves. Asterisks and yellow arrows respectively indicate the ectopic sorting of spinal motor neuron axons and somata from the spinal cord. Scale bars: 25 μm. (D-K) Quantifications of pMN and sMN defects in embryos and larvae immunolabelled in panel C. Mean number of branches (D) and truncated CaP axons (E) per embryo. Mean number of split/misguided dorsal nerves (F), misrouted rostral nerves (G), missing dorsal nerves (H) and defasciculated rostral nerves (I) per larva. Quantifications were performed on 24 spinal hemisegments located around the yolk tube per embryo or larva. Box and Whiskers graphs. ***$p \leq 0.001$; ns: non-significant; Kruskal–Wallis ANOVA test with Dunn's post test. Whiskers indicate the Min/Max values. (J-K) Percentage of larvae with ectopic sorting of secondary motor neuron (sMN) axons (J) or somata (K) from the spinal cord. ***$p \leq 0.001$. Chi^2 test.

Figure 7. TTLL6 and TTLL11 play non-redundant roles in spinal motor axon outgrowth and navigation. (A) Rescue and cross-rescue experiments of *TTLL6* morphant phenotypes by co-injection of mouse *TTLL6* or *TTLL11* transcripts. (B) Reciprocal rescue and cross-rescue experiments of *TTLL11* morphant phenotypes by co-injection of mouse *TTLL11* or *TTLL6* transcripts. (A-B) Upper panels: Overall

morphology of 72-hpf control, morphant and rescued larvae. Scale bars: 250 µm. Middle panels: immunolabelling of pMN axons with Znp-1 antibody in 26-hpf embryos injected with control (MO^{Ctl}, n=19), *TTLL6* (MO^{TTLL6}, n=22), *TTLL11* (n=19) morpholinos or co-injected with MO^{TTLL6} or MO^{TTLL11} and mouse *TTLL6* or *TTLL11* mRNA (MO^{TTLL6} + $mRNA^{TTLL6}$, n=20; MO^{TTLL6} + $mRNA^{TTLL11}$, n=21; MO^{TTLL11} + $mRNA^{TTLL11}$, n=19; MO^{TTLL11}+ $mRNA^{TTLL6}$, n=18). Arrows and asterisks respectively indicate hyper-branched and truncated CaP axons. Bottom panels: Immunolabelling of sMN axons with Zn-5 and GFP antibodies in 72-hpf Tg(*Hb9*:GFP) larvae injected with control (MO^{Ctl}, n=22), *TTLL6* (MO^{TTLL6}, n=22), *TTLL11* (n=21) morpholinos or co-injected with MO^{TTLL6} or MO^{TTLL11} and mouse *TTLL6* or *TTLL11* mRNA (MO^{TTLL6} + $mRNA^{TTLL6}$, n=19; MO^{TTLL6} + $mRNA^{TTLL11}$, n=22; MO^{TTLL11} + $mRNA^{TTLL11}$, n=17; MO^{TTLL11} + $mRNA^{TTLL6}$, n=22). Dotted lines delineate lateral myosepta. Full arrowheads and full arrows respectively indicate normal rostral and dorsal nerves. Empty arrowheads and empty arrows respectively point at misguided rostral and dorsal projections. Middle and bottom panels: lateral views of the trunk, anterior to the left. Scale bars: 25 µm. (C-J) Quantifications of pMN and sMN defects in embryos and larvae immunolabelled in panels A and B. Mean number of branches (C) and truncated CaP axons (D) per embryo. Mean number of split/misguided dorsal nerves (E), misrouted rostral nerves (F), missing dorsal nerves (G) and defasciculated rostral nerves (H) per larva. Quantifications were performed on 24 spinal hemisegments located around the yolk tube per embryo or larva. Box and Whisker graphs. * $p \leq 0.05$; *** $p \leq 0.001$; ns: non-significant; One-Way ANOVA test with Bonferroni's post-test (C, F) or Kruskal–Wallis ANOVA test with Dunn's post test (D-E, G-H). Whiskers indicate the Min/Max values. Percentage of

larvae with ectopic sorting of sMN axons (I) and somata (J) from the spinal cord. **p≤0.01; ***p≤0.001; ns: non-significant. Chi^2 test.

Figure 8. Selective rescue of motor neuron and locomotion defects associated with *p60-katanin* partial knockdown by TTLL6 overexpression. (A) Upper panels: Tracking analysis of 72-hpf larvae injected with a control morpholino (MO^{Ctl}, n=30), 1.3 pmol of MO^{p60Kat} ($MO^{p60Kat/1.3pmol}$, n=30) or co-injected with 1.3 pmol of MO^{p60Kat} and mouse *TTLL6* ($MO^{p60Kat/1.3pmol}$ + $mRNA^{TTLL6}$, n=30) or *TTLL11* mRNAs ($MO^{p60Kat/1.3pmol}$ + $mRNA^{TTLL11}$, n=30) in a touch-evoked escape response test. Each line represents the trajectory of one larva after touch stimulation while the distance between two dots indicate the distance covered by a larva between two consecutive frames. Scale bar: 5 mm. Middle panels: Immunolabelling of pMN axons with Znp-1 antibody in 26-hpf embryos injected with control morpholino (MO^{Ctl}, n=20), 1.3 pmol of MO^{p60Kat} ($MO^{p60Kat/1.3pmol}$, n=21) or co-injected with $MO^{p60Kat/1.3pmol}$ and mouse *TTLL6* ($MO^{p60Kat/1.3pmol}$ + $mRNA^{TTLL6}$, n=19) or *TTLL11* mRNA (MO^{p60Kat} + $mRNA^{TTLL11}$, n=16). Arrows indicate hyper-branched CaP axons. Bottom panels: Immunolabelling of sMN axon tracts using Zn-5 and GFP antibodies in 72-hpf Tg(*Hb9*:GFP) larvae injected with a control morpholino (MO^{Ctl}, n=20), 1.3 pmol of MO^{p60Kat} ($MO^{p60Kat/1.3pmol}$, n=20) or co-injected with $MO^{p60Kat/1.3pmol}$ and mouse *TTLL6* ($MO^{p60Kat/1.3pmol}$ + $mRNA^{TTLL6}$, n=19) or *TTLL11* (MO^{p60Kat} + $mRNA^{TTLL11}$, n=20) mRNAs. Dotted lines delineate lateral myosepta. Full arrowheads and full arrows respectively point at normal rostral and dorsal projections. Empty arrowheads and empty arrows respectively indicate misguided rostral and dorsal tracts. Middle and lower panels: Lateral views of the trunk, anterior to the left. Scale bar: 25 µm. (B-C) Mean swimming distance (B) and speed (C) of the set of larvae tracked in panel A.

Box and Whisker graphs. ***p≤0.001; ns: non-significant (p>0.05); Kruskal–Wallis ANOVA test with Dunn's post test. Whiskers indicate the Min/Max values. (D-F) Quantifications of pMN and sMN defects in embryos and larvae immunolabelled in panel A. Mean number of branches (D) per embryo. Mean number of split/misguided dorsal nerves (E) and misrouted rostral nerves (F) per larva. Quantifications were performed on 24 spinal hemisegments located around the yolk tube per embryo or larvae. Box and Whisker graphs; *p≤0.05; **p≤0.01; ***p≤0.001; ns: non-significant; One-Way ANOVA test with Bonferroni's post-test (D) or Kruskal–Wallis ANOVA test with Dunn's post test (E-F). Whiskers indicate the Min/Max values.

Figure 9: TTLL6 fails to rescue the axon pathfinding errors and locomotor deficits of *p60-katanin* null mutants. (A) Immunolabelling of sMN axon tracts with Zn-5 antibody in 72-hpf *katna1*$^{+/+}$ (n= 57), *katna1*$^{-/-MZ}$ (n= 61) and *katna1*$^{-/-MZ}$ larvae injected with the transcripts encoding mouse TTLL6 (n= 56), TTLL11 (n= 54) or human p60-katanin (n= 69). Lateral views of the trunk, anterior to the left. Right panels are higher magnifications of the boxed region in left panels. Arrows point at split/misguided dorsal nerves. Scale bars: 25 μm. (B-C) Quantifications of dorsal nerve defects. Quantifications were performed on 24 spinal hemisegments located around the yolk tube of each larva immunolabelled in panel A. (B) Percentage of larvae with dorsal nerve defects. (C) Mean number of split/misguided dorsal nerves per larva. (D) Mean larval swimming speed in the escape-touch response test. Swimming speed values were extracted from tracking analysis of 72-hpf *katna1*$^{+/+}$ (n= 65), *katna1*$^{-/-MZ}$ (n= 74) and *katna1*$^{-/-MZ}$ larvae injected with the mRNAs encoding mouse TTLL6 (n= 78), TTLL11 (n= 78) or human p60-katanin (n= 47). (E) Percentage of larave showing a curved-tail phenotype. (C-D) Box and Whisker

graphs; ***p≤0.001; ns: non-significant (p>0.05). Kruskal–Wallis ANOVA test with Dunn's post test. Whiskers indicate the Min/Max values. (B, E) **p≤0.01; ***p≤0.001; ns: non-significant (p>0.05). Chi^2 test.

Table 1: Primers used for qPCR analysis

Gene	Forward sequence (5'-3')	Reverse sequence (5'-3')
spast	AAGGCAGACAGAGCCAGAAAA	TGAAAGCAGATTGCCCAGAAG
katnal2	GAGGCTGCCAAGCGATTAGT	GGCGACAGGATTCCAGTGAA
Fign	CCCGCACAAGCATTCATCAG	CCACTGCATCTTTAAGCCTGT
Fignl1	TCCAGGCACTGGTAAAACCC	CCTTCCCCGACCCATTTTGA
katnal1	GTCTGCAGAGATGCGTCGAT	ATGGTGACCGGCATCTGAAG
vps4a	AGCATCTCATGGGTGCGATT	GAGCTTCTTTGGCTCCCTCC
lsm12b	GAGACTCCTCCTCCTCTAGCAT	GATTGCATAGGCTTGGGACAAC

Figure S1. *p60-katanin* transcript is enriched in the zebrafish developing nervous system

Whole-mount *in situ* hybridisation with *p60-katanin* sense (upper panel) and antisense (bottom panel) riboprobes at 18 somites and 24 hours post-fertilisation (hpf). Lateral views of the embryos, anterior to the left. *p60-katanin* is highly enriched in the developing nervous system at both 18 somites and 24 hpf, two stages at which pMN and sMN axons exit the spinal cord to navigate towards their muscle targets. Scale bars: 200 μm.

Figure S2. *p60-katanin* knockdown using the published morpholino MO^{katna1aug1} induces identical spinal motor axon defects to MO^{p60Kat} morpholino. (A) Immunolabelling of sMN tracts in 72 hours-post-fertilisation (hpf) transgenic Tg(*Hb9*:GFP) larvae injected with control (n=40) or MO^{katna1aug1} (n=40) morpholinos, using Zn-5 and GFP antibodies. Lateral views of the trunk, anterior to the left. Bottom panels represent higher magnifications of top panels. Dotted lines delineate lateral myosepta. Full arrowheads and full arrows respectively point at normal rostral and dorsal nerves. Empty arrowheads show misguided rostral nerves. Asterisks indicate ectopic sorting points of sMN axons from the spinal cord. (B-C) Quantifications of sMN defects in larvae immunolabelled in panel A. Mean number of missing dorsal nerves (B) and misguided rostral nerves (C) per larva. Quantifications were performed on 24 spinal hemisegments located around the yolk tube per larva. Box and Whisker graphs. ***p≤0.001; Mann Whitney test. Whiskers indicate the Min/Max values.

Figure S3: Overexpression of human p60-katanin fails to rescue spinal motor axon outgrowth and pathfinding defects of spastin-depleted larvae. (A) Mean number of shorter CaP axons per embryo in 26-hpf embryos injected with control (COMO*sp*^{ATG1}, n=10), spastin morpholino (MO*sp*^{ATG1}, n=10) or co-injected with MO*sp*^{ATG1} and human *KATNA1* mRNA (n=10). (B-D) Mean number of misrouted rostral nerves (i.e., caudally targeted; B), missing rostral nerves (C) and missing dorsal nerves (D) per larva in 72-hpf larvae injected with control (COMO*sp*^{ATG1}, n=29), spastin morpholino (MO*sp*^{ATG1}, n=30) or co-injected with MO*sp*^{ATG1} and human *KATNA1* mRNA (n=29). (A-D) Quantifications were performed on 24 spinal hemisegments located around the yolk tube per embryo or larva. Box and Whisker graphs. ***p≤0.001; ns: non-significant; One-Way ANOVA test with Bonferroni's post-test (A, C) or Kruskal–Wallis ANOVA test with Dunn's post test (B, D). Whiskers indicate the Min/Max values.

Figure S4: Maternal zygotic *katna1* mutants show defective inflation of the swimming bladder. Gross morphology of 6-days-post-fertilisation (dpf) control (*katna1*$^{+/+}$) and maternal zygotic mutant (*katna1*$^{-/-}$*MZ*) larvae. Insets are higher magnifications of the swimming bladder framed by dotted boxes. Maternal zygotic *katna1* mutants failed to inflate their swimming bladder. Scale bars: 0.5 mm.

Figure S5: Zebrafish *katna1* mutants display misguided rostral motor nerves. (A-B) Quantifications of rostral nerve defects in 72-hpf controls (*katna1*$^{+/+}$, n=34), and heterozygous (*katna1*$^{+/-}$, n=53), homozygous zygotic (*katna1*$^{-/-}$*Z,* n=33) and maternal zygotic (*katna1*$^{-/-}$*MZ,* n=12) *katna1* mutant larvae using Zn-5 antibody. (A) Percentage of larvae with rostral nerve defects. *p≤0.05; ***p≤0.001; Chi2 test. (B) Mean number of misguided rostral projections. Box and Whisker graphs. *p≤0.05; ns: non-significant; Kruskal–Wallis ANOVA test with Dunn's post test. Whiskers indicate the Min/Max values.

Movies 1, 2: *p60-katanin* knockdown strikingly impairs spinal motor axon navigation

Movie 1: Time-lapse videomicroscopy of motor axon outgrowth in control Tg(*Hb9*:GFP) larvae. Frames were acquired with a spinning disk microscope and a 20x objective every 8 minutes from 20 to 72 hpf.

Movie 2: Time-lapse videomicroscopy of motor axon outgrowth in MO^{p60Kat}-injected Tg(*Hb9*:GFP) larvae. Frames were acquired with a spinning disk microscope and a 20x objective every 8 minutes from 20 to 72 hpf.

Movies 3, 4: *p60-katanin* knockdown leads to the abnormal splitting of the dorsal nerve.

Movie 3: Time-lapse videomicroscopy of dorsal motor nerve outgrowth in control Tg(*Hb9*:GFP) larvae. Frames were acquired with a spinning disk microscope and a 40x objective every 8 minutes from 40 to 72 hpf.

Movie 4: Time-lapse videomicroscopy of dorsal motor nerve outgrowth in MO^{p60Kat}-injected Tg(*Hb9*:GFP) larvae. Frames were acquired with a spinning disk microscope and a 40x objective every 8 minutes from 40 to 72 hpf.

Movies 5-10: The swimming deficit of *p60-katanin* morphants is rescued by overexpression of human *KATNA1* transcript but not by zebrafish *spastin* mRNA.

Movie 5: Touch-evoked mobility of 72-hpf control larvae.

Movie 6: Touch-evoked mobility of 72-hpf $MO^{p60Kat/1.3pmol}$-injected larvae.

Movie 7: Touch-evoked mobility of 72-hpf larvae injected with $MO^{p60Kat/1.3pmol}$ and 120 pg of human *KATNA1*mRNA.

Movie 8: Touch-evoked mobility of 72-hpf $MO^{p60Kat/3.4pmol}$-injected larvae.

Movie 9: Touch-evoked mobility of 72-hpf larvae injected with $MO^{p60Kat/3.4pmol}$ and 180 pg of human *KATNA1* mRNA.

Movie 10: Touch-evoked mobility of 72-hpf larvae injected with $MO^{p60Kat/1.3pmol}$ + 150 pg of zebrafish *spastin* mRNA.

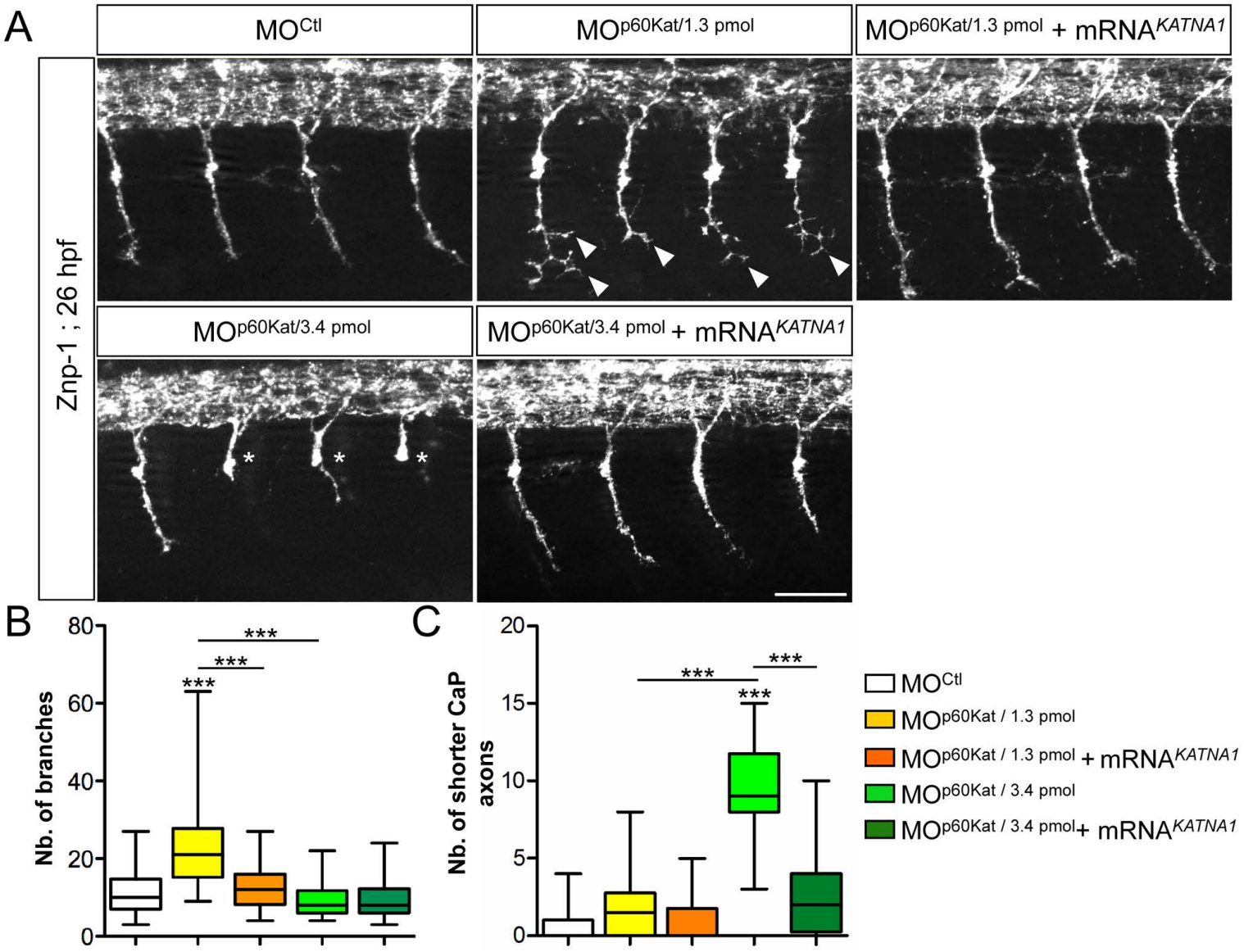

Figure 1

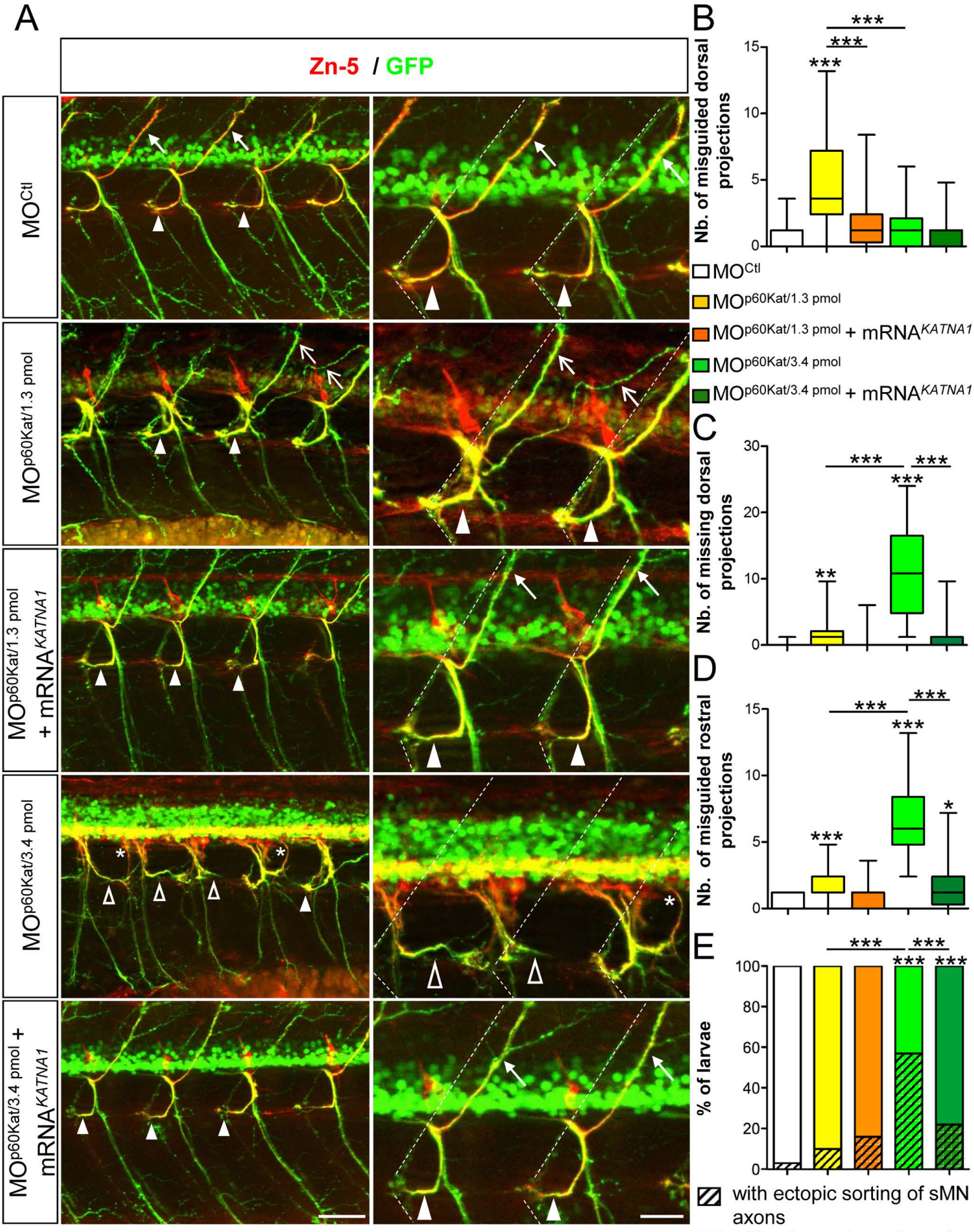

Figure 2

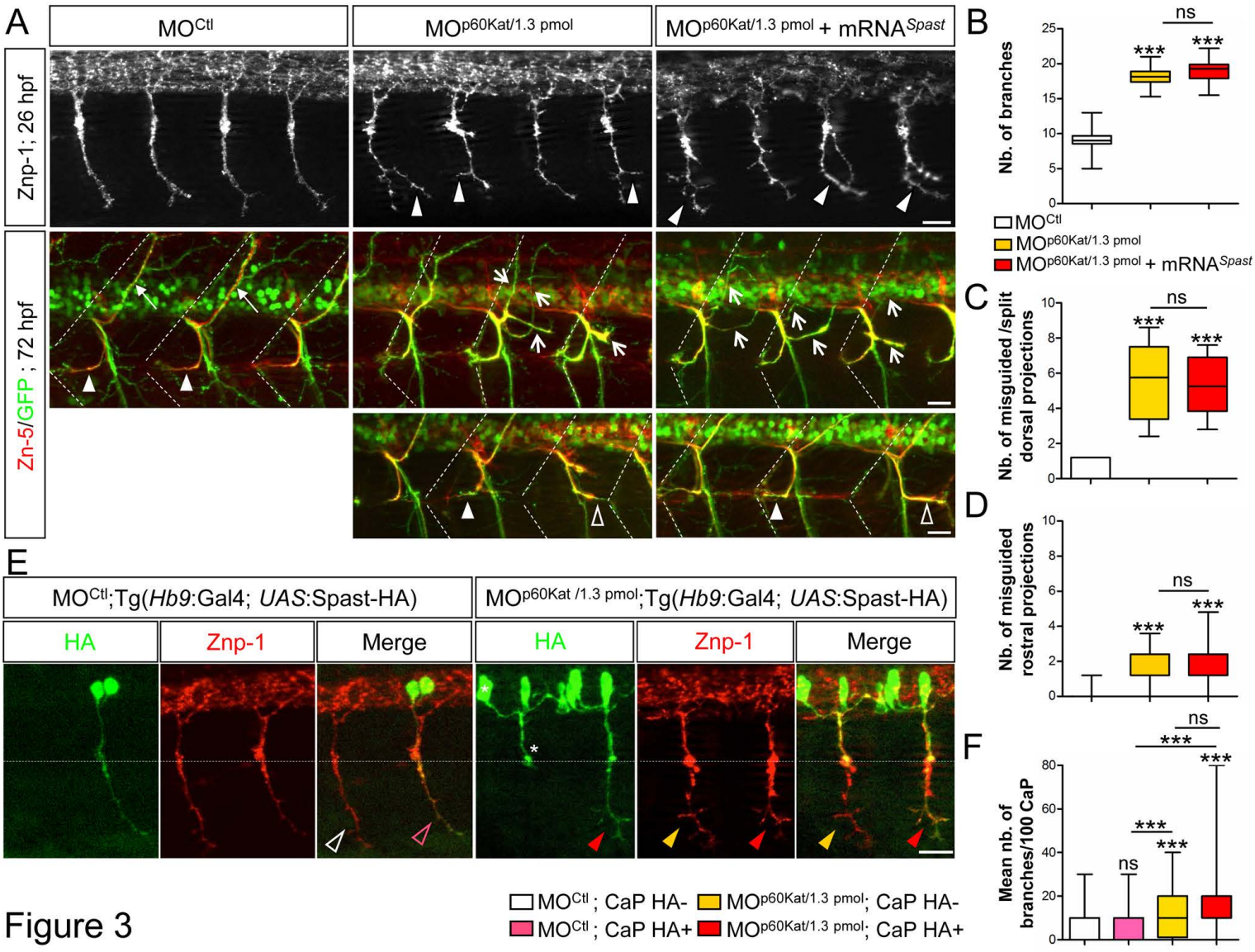

Figure 3

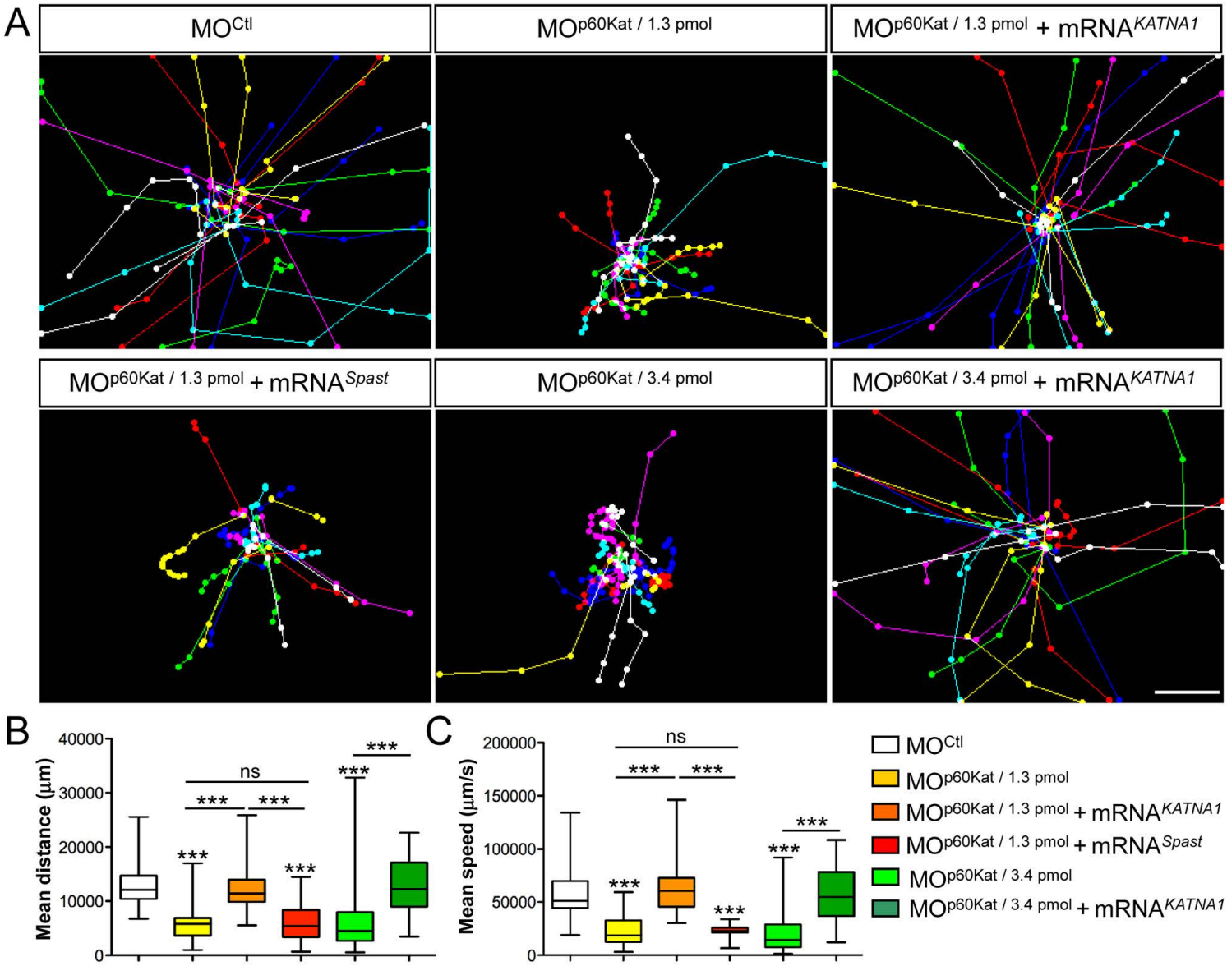

Figure 4

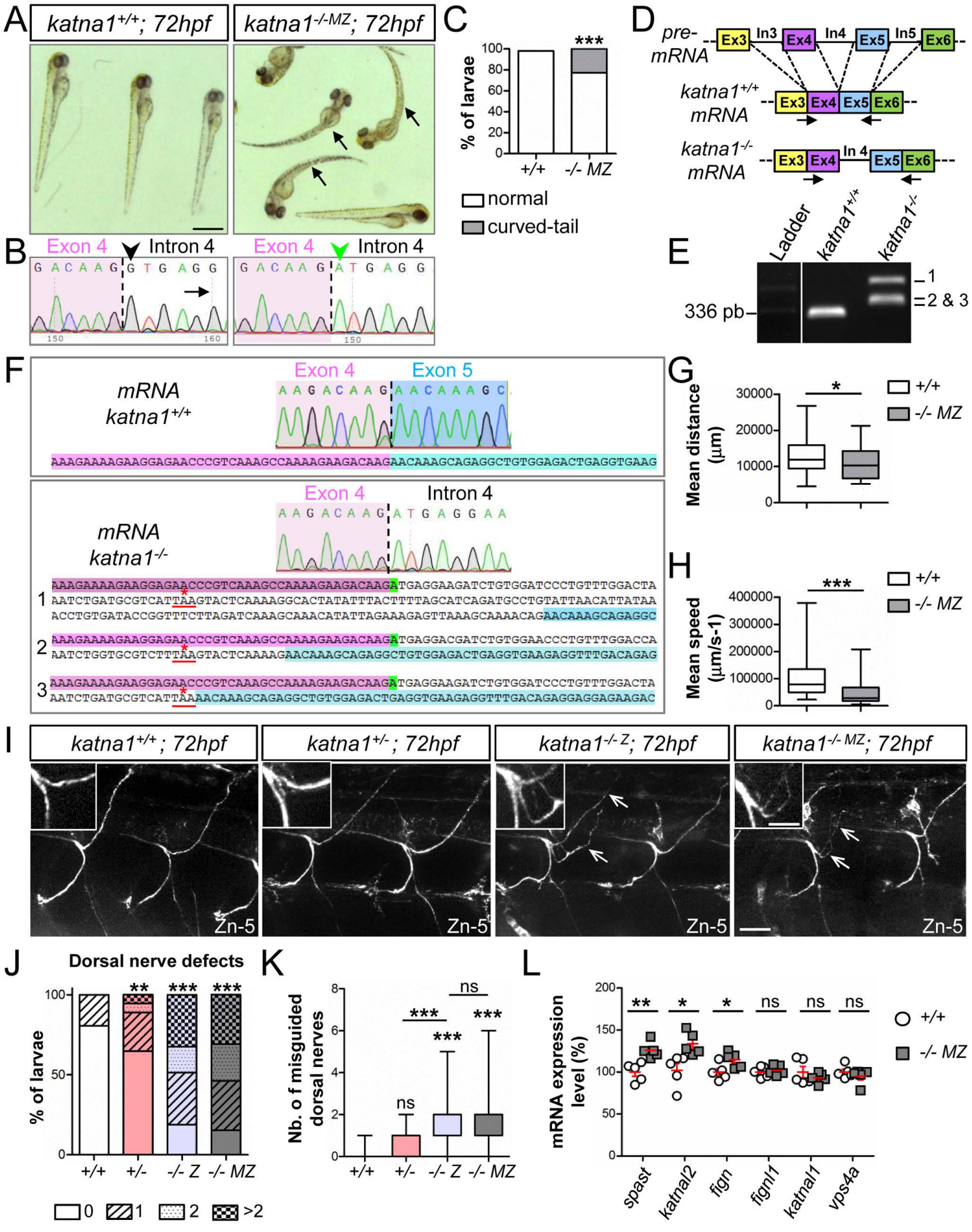

Figure 5

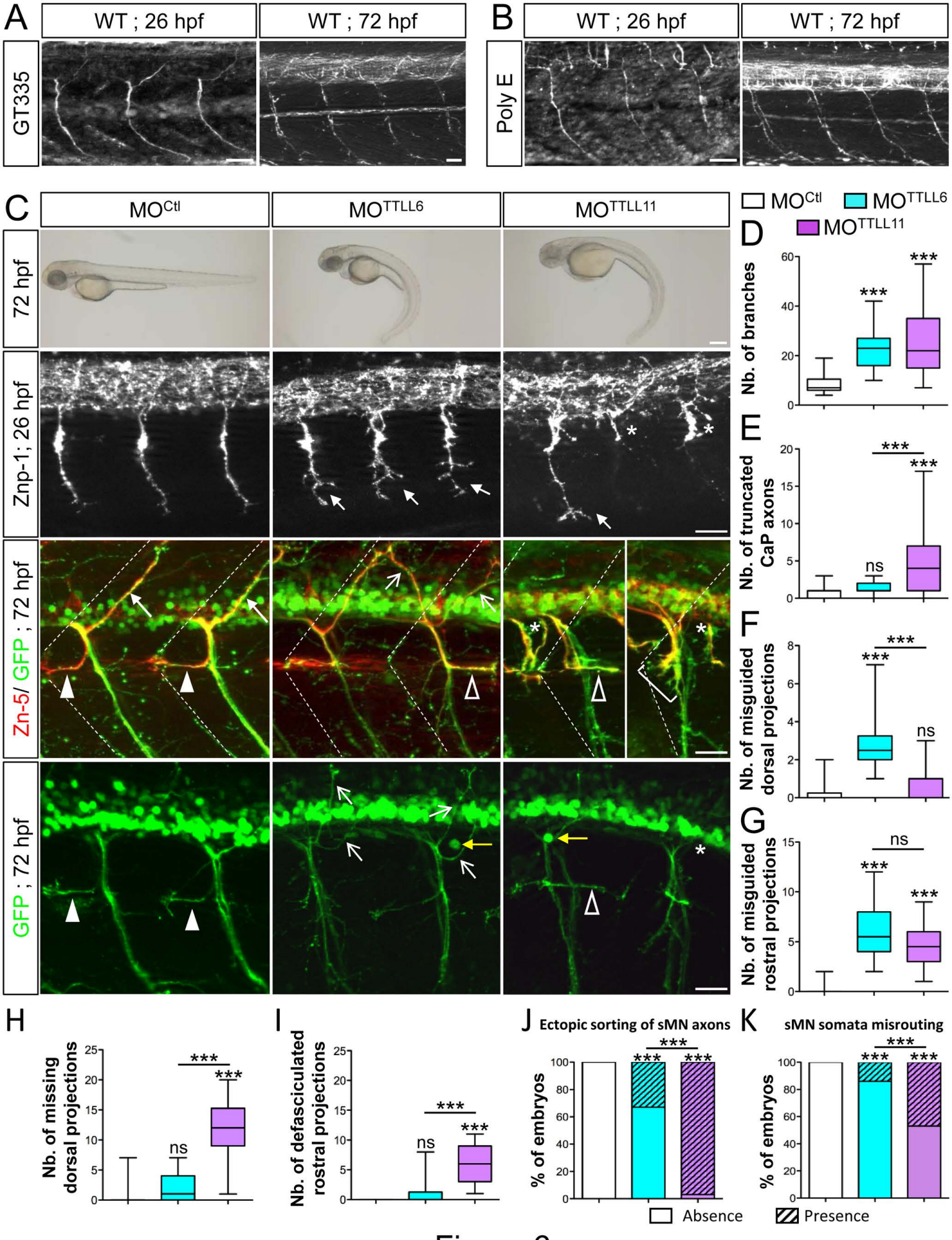

Figure 6

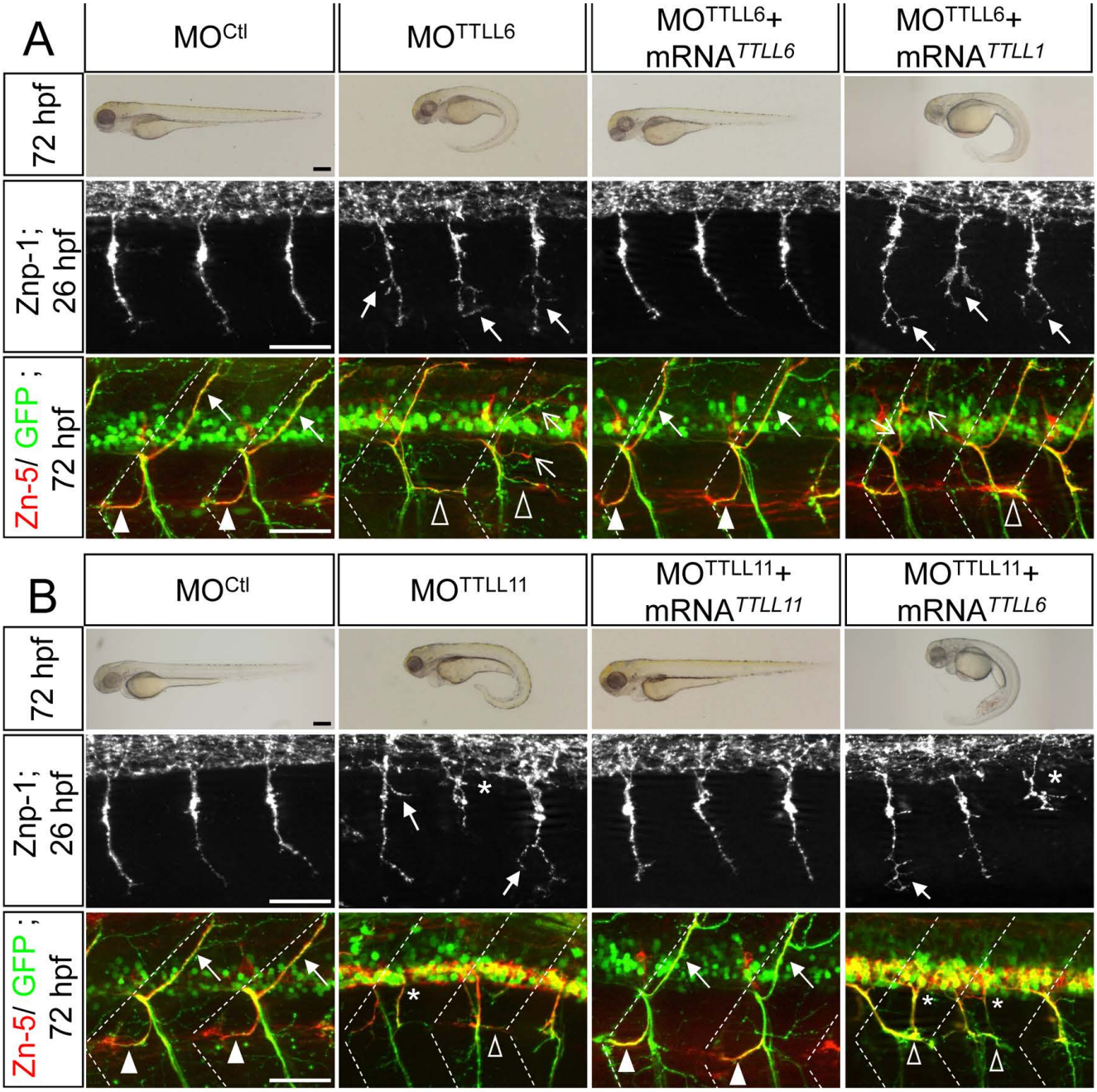

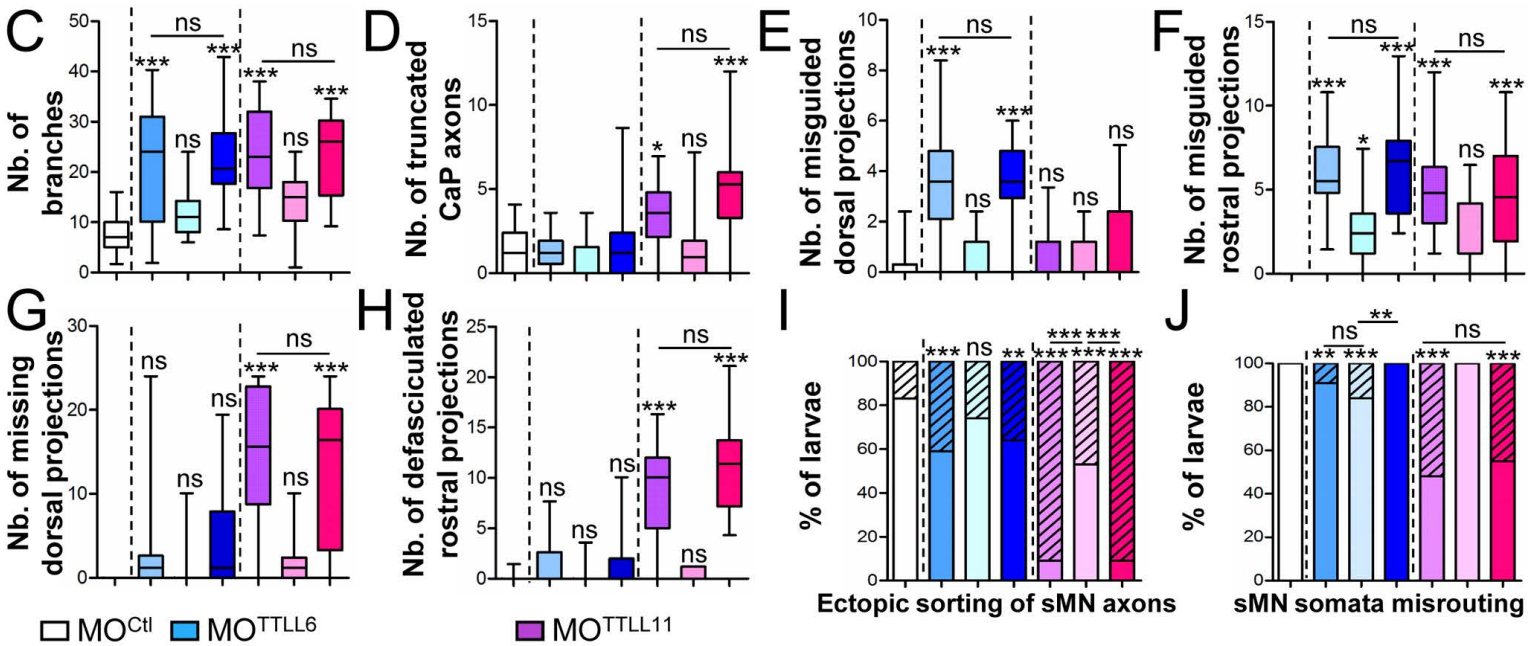

Figure 7

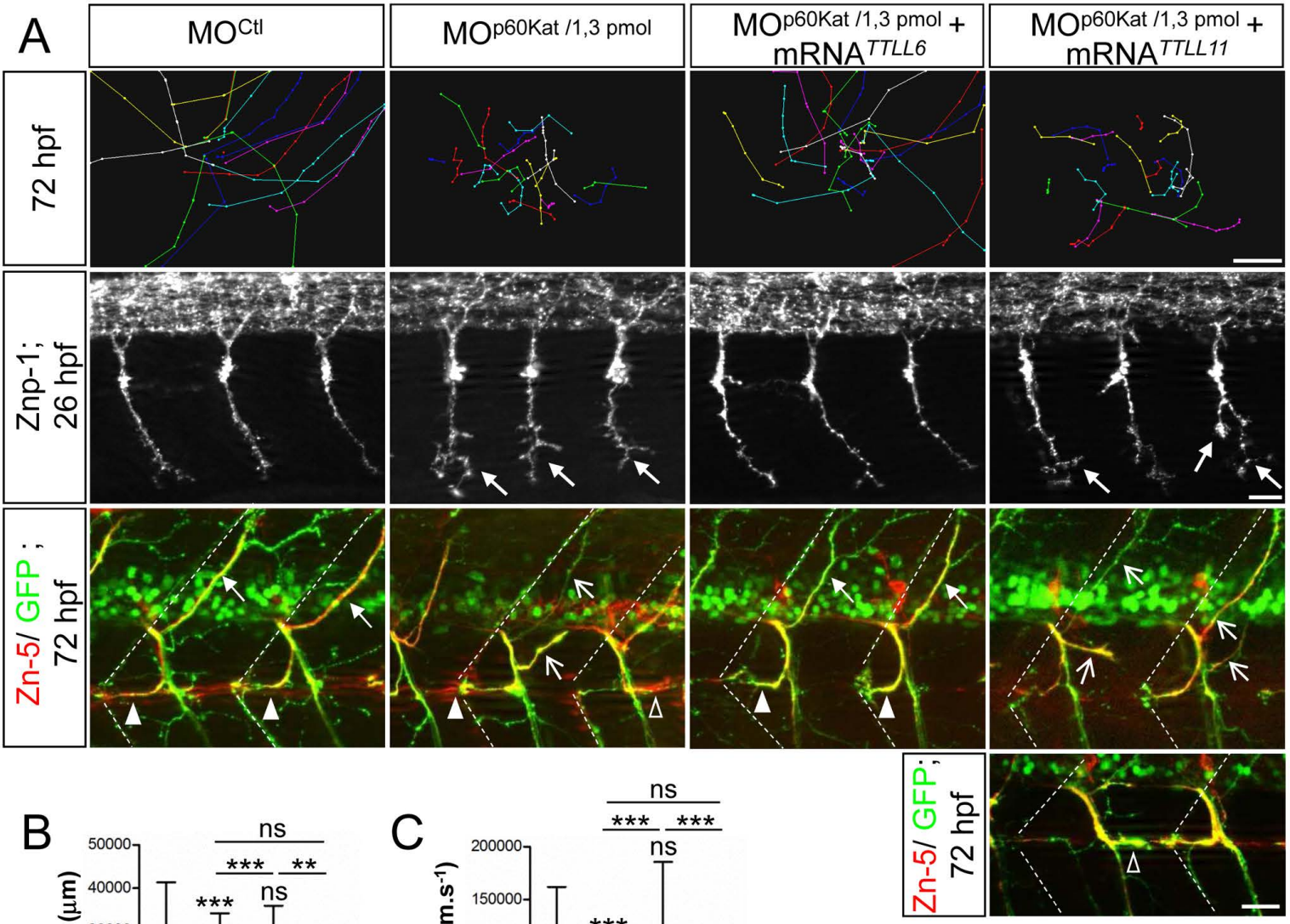

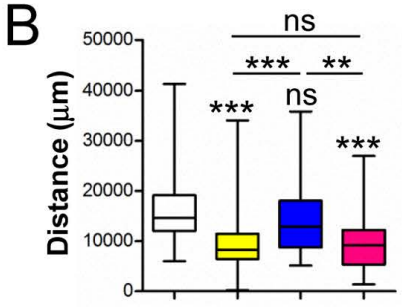

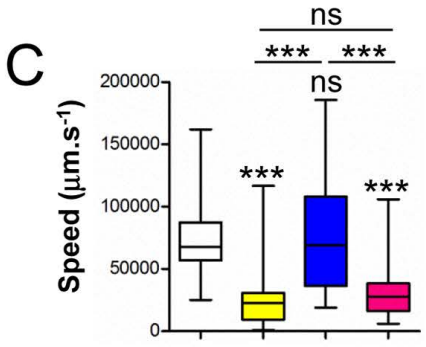

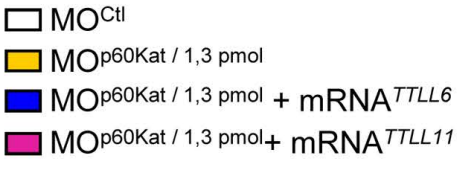

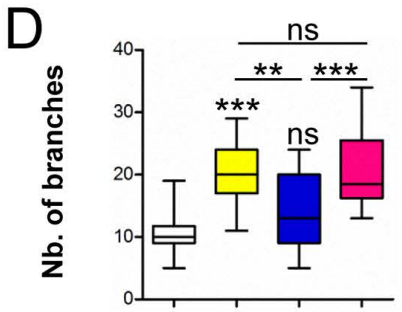

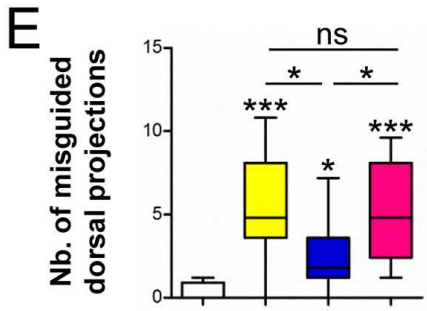

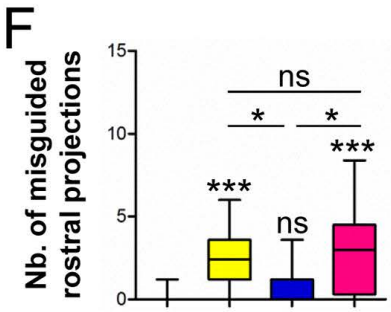

Figure 8

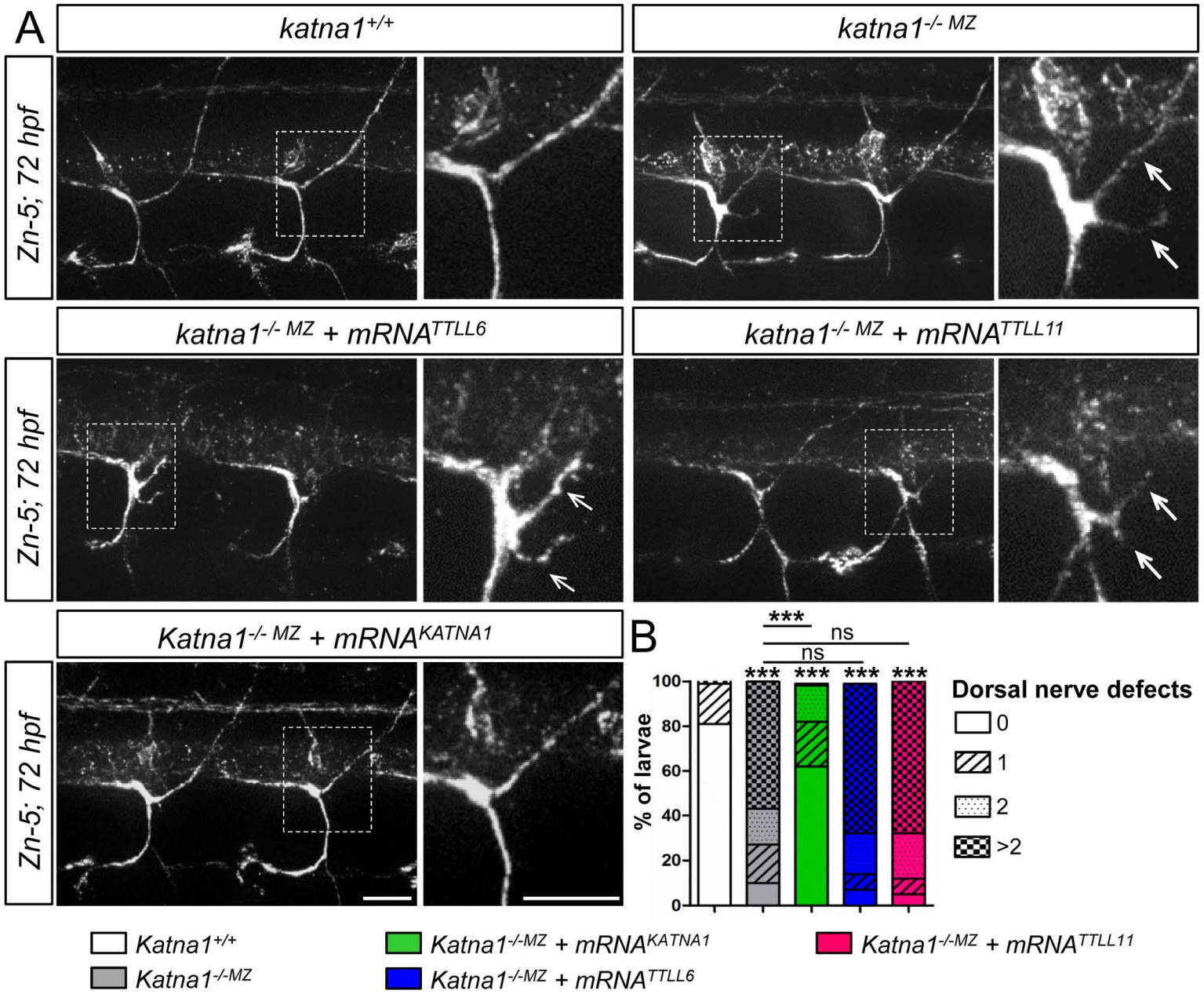

Figure 9